

**SINGLE MOLECULE STUDIES OF DIFFUSION DYNAMICS IN
POLYMER THIN FILMS NEAR T_g**

A thesis
Presented to
The Academic Faculty

by

Kewei Xu

In Partial Fulfillment
of the Requirements for the Degree
Master of Science in Chemistry

Georgia Institute of Technology
August 2007

**SINGLE MOLECULE STUDIES OF DIFFUSION DYNAMICS IN
POLYMER THIN FILMS NEAR T_g**

Approved by:

Dr. Robert Dickson, Advisor
School of Chemistry and Biochemistry
Georgia Institute of Technology

Dr. Mohan Srinivasarao
School of Polymer, Textile & Fiber Engineering
Georgia Institute of Technology

Dr. Haskell W. Beckham
School of Polymer, Textile & Fiber Engineering
Georgia Institute of Technology

Date Approved: July 2, 2007

ACKNOWLEDGEMENTS

First I would like to thank my advisor, Professor Robert Dickson, for his support and guidance while conducting this research. I would also like to thank all the members of the Dickson group, especially Andrew Bartko, Jung-Cheng Hsiang and Yasuko Antoku. Additionally I would like to thank my committee and to all others that assisted me during my time at Georgia Tech.

Finally I want to thank my wife, Yu Yang, for her encouragement, support and confidence in me.

TABLE OF CONTENTS

	Page
ACKNOWLEDGEMENTS	iv
LIST OF TABLES	vi
LIST OF FIGURES	vii
SUMMARY	ix
<u>CHAPTER</u>	
1 Introduction	1
1-1 Translational-orientational diffusion in polymer near Tg	1
1-2 Single molecule fluorescence microscopy	5
2 Experimental Section	11
2-1 TIR fluorescence microscopy setup	11
2-2 Polymer thin film near the glass transition temperature	13
3 Results and discussion	15
3-1 Emission pattern fitting to determine the orientation of single molecules	15
3-2 Single molecule tracking	21
3-3 Orientational and translational diffusion results	22
4 3-detector methods to determine the 3-D orientation of single molecules	38
4-1 Different methods to determine the 3-D orientation of single molecules	38
4-2 3-Detector method experiment set up	44
4-3 Result and discussion	46
REFERENCES	53

LIST OF TABLES

	Page
Table 3.1: Temperature dependence, population of moving molecules, D and different translational diffusion model in PIPA thin films.	36

LIST OF FIGURES

	Page
Figure 1.1: Thermodynamics (a) and dynamics (b) properties of super-cooled liquid.	2
Figure 1.2: Conventional experiment setups used for single molecule fluorescence microscopy.	7
Figure 2.1: TIRFM experimental set up.	12
Figure 2.2: Chemical structure of PIPA and Alexa [®] 514.	13
Figure 3.1: Typical CCD images of single molecules.	17
Figure 3.2: Examples of fits of simulated images to experimental emission patterns.	18
Figure 3.3: Orientational libraries for a specific set of optical conditions.	20
Figure 3.4: Typical orientation trajectories of single dye molecules in PIPA thin films.	23
Figure 3.5: Autocorrelation curves of the molecular motions.	24
Figure 3.6: Histogram of exponential decay constants for molecules' rotational autocorrelations observed within PIPA films at different temperatures.	27
Figure 3.7: Mean square displacements (MSD) as a function of time for different types of diffusion models.	29
Figure 3.8: A typical data set of single Alexa dye molecules' translational motions in thin PIPA films at $T = 55$ °C.	31
Figure 3.9: Schematic illustration of regions of spatially heterogeneous dynamics of polymer near T_g .	31
Figure 3.10: Mean square displacement (MSD) comparison of single dye molecules (Alexa) in PIPA thin films at different temperatures.	33
Figure 3.11: Confined diffusion fits for the single dye molecules (Alexa) translational diffusion in PIPA thin films at $T = 5$ °C and 10 °C	33
Figure 3.12: Normal diffusion fits for the single dye molecules (Alexa) translational diffusion in PIPA thin films at $T = 40$ °C, 50 °C, and 55 °C.	34
Figure 3.13: Individual molecules MSD vs. time curves.	36
Figure 4.1: Schematic experimental setup	39

Figure 4.2: Schematic figure of a transition dipole orientation.	41
Figure 4.3: Experiment setup for comparing 3D methods of determining the orientation of single molecules.	45
Figure 4.4: Typical data from pattern fit method and three-detector method.	47
Figure 4.5: The 3-detector data at different time resolution.	49
Figure 4.6: Orientation fit result comparison for different methods.	50

SUMMARY

For polymers near the glass transition, the dynamics in some regions can be orders of magnitude different compared with the dynamics in other regions only a few nanometers away, so called spatial heterogeneity [1]. In this thesis, single molecule fluorescence microscopy as a powerful tool, was applied to study the spatially heterogeneous dynamics, both orientational and translational, within the polymer matrix near the glass transition temperature. With our total internal reflection fluorescence microscopy (TIRFM) methods, many individual fluorescent dye molecules embedded in the poly (isopropyl acrylate) (PIPA) thin films can be simultaneously excited. Their emission patterns are analyzed using our orientation determination methods [2] to give the true 3D orientational trajectories of the individual molecules. At $T_g < T < 1.2 T_g$, single molecule tracking was used to study the dye molecules' translational diffusion. Results show that, below $1.1 T_g$, the probe molecules are in the confined flow region [3]; at $T > 1.1 T_g$, the diffusion follows normal diffusion model; at $T = 1.2 T_g$, although the statistical results shows that normal random walk behavior is followed, the individual molecules still show different diffusion behaviors, clear evidence of the spatial heterogeneity that still exists at this temperature.

The second part of this thesis is a development of the 3-detector method to determine the 3D orientation of single molecules [4]. This method is based on the work proposed by Fourkas [4] in 2001. Results utilizing this experimental setup are compared with our emission pattern fitting methods. The results show that, with a little bit higher error range (10° in θ , 20° in φ), the 3-detector method can give agreeable orientation

fittings, further more, with higher time resolution of < 10 ms. This 3-detector method is useful and can be applied to study the fast orientation dynamics in different systems.

CHAPTER 1

INTRODUCTION

1-1 Translational-orientational diffusion in glassy state polymer

One of the most challenging problems in polymer and materials science is an understanding of the glass transition of polymers. Because of the technical and scientific importance of the glass transition, the research on polymers near the glass transition has enormously intensified in the past few years [5]. The glass transition is different from solidification by crystallization. The latter is a phase transition with a well defined thermodynamics transition temperature, the crystallization temperature. But polymers, or so-called super-cooled liquids, undergo significant changes in both thermodynamic and dynamic properties. At high temperature these materials are in the rubbery state and are viscous liquids. The viscosity increases as cooling proceeds down to the glass transition temperature T_g . The increase of viscosity is continuous and can be more than 10 orders of magnitude near T_g in comparison with the viscosity in the rubbery state [6].

Fig 1.1 (a) [1] is a plot of the specific volume, V_{SP} , as a function of temperature for a typical liquid that undergoing different thermodynamic changes. When cooling from high temperature, a “normal” liquid may crystallize at T_m . The changes in V_{SP} on cooling is one convenient way to define T_g . T_g is an important material property; it is the most useful parameter in estimating the mechanical properties of a glass forming material. Fig 1.1 (b) shows some dynamic characteristics of supercooled liquids. Viscosity is a macroscopic character of the dynamics of a supercooled liquid, and is dramatically increased as T_g is approached. For o-terphenyl, the viscosity increases 11 orders of magnitude from room temperature down to T_g [6]. The rotational correlation time at T_g is

about 10^4 s [7]. This is an extremely long time compared to the pico-second range rotation correlation times observed in a “typical” liquid [7].

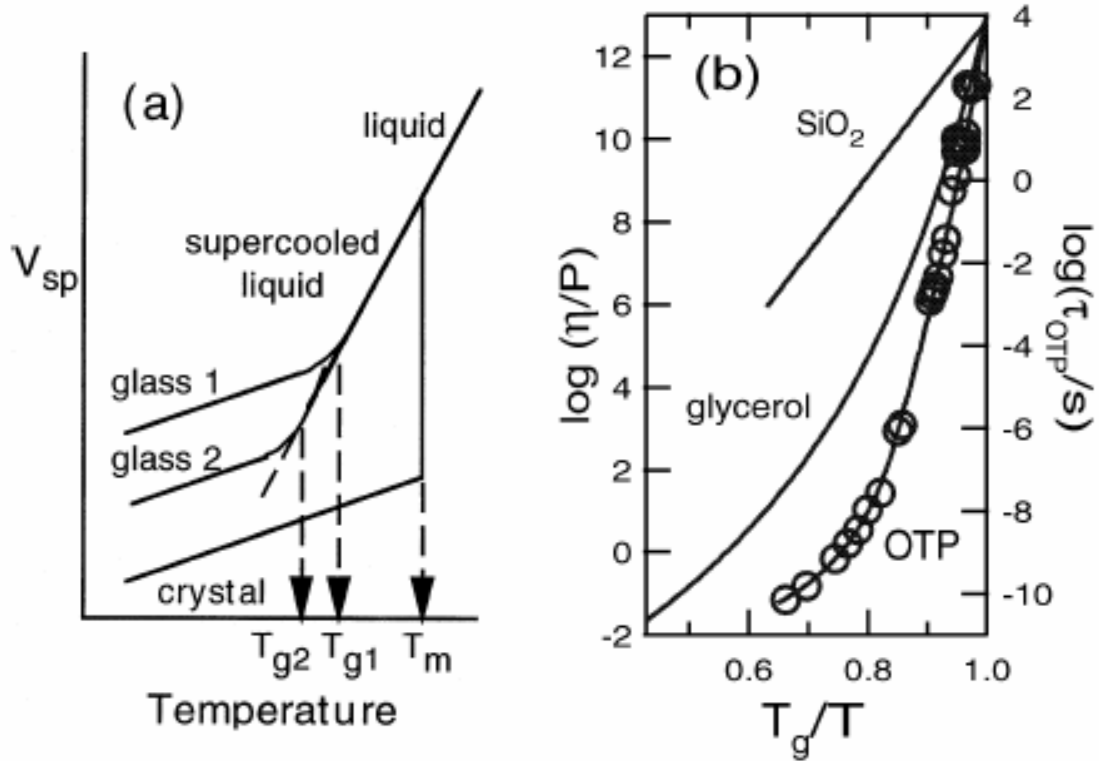


Fig 1.1 Thermodynamics (a) and rotational dynamics (b) properties of supercooled liquids. Reproduced from Ref [1]

(a) The specific volume V_{SP} as a function of temperature for a typical liquid.

(b) (solid lines) Viscosity of three different liquids.

(open circles) NMR measurement of the rotational correlation times for o-terphenyl.

It is useful to classify supercooled liquids between “strong” and “fragile” behavior. See the left figure in Fig 1.1, liquids like o-terphenyl, which show a strong non-Arrhenius temperature dependence as T_g is approached, have been characterized by Angell as “fragile” liquids [8]. Materials like SiO_2 , with Arrhenius temperature dependence for $\eta(T)$, are known as “strong”. A very interesting phenomenon was uncovered on the deeply supercooled fragile liquids by nuclear magnetic resonance

(NMR) experiments and forced Rayleigh scattering experiments [7, 9, 10], the translational motion is “enhanced” more than 100 times relative to the orientational motion, so-called translation-rotation diffusion paradox [11].

It has become traditional to interpret translational and rotational diffusion of individual molecules in liquids by the Stokes-Einstein-Debye model [12-14]. This model predicts that the translational and rotational diffusion coefficients can be expressed as following equations:

$$D_{trans} = \frac{k_B T}{6\pi\eta R} \quad (1a)$$

$$D_{rot} = \frac{k_B T}{8\pi\eta R^3} \quad (1b)$$

where k_B is Boltzmann’s constant, η is the bulk viscosity, and R is the radius of the molecular sphere. D_{trans} and D_{rot} measure the rates of increase of mean-square positional displacement, $\langle(\delta r)^2\rangle$ and angular displacement, $\langle(\delta\theta)^2\rangle$ of the Brownian particles:

$$\langle(\delta r)^2\rangle \cong 6D_{trans}\delta t \quad (2a)$$

$$\langle(\delta\theta)^2\rangle \cong 4D_{rot}\delta t \quad (2b)$$

The Stokes-Einstein-Debye model is remarkably successful in rationalizing data for a wide range of liquids in their higher temperature range ($T \geq T_m$), and in the moderately supercooled temperature range ($T \geq 1.2 T_g$) [12-14]. The temperature variations of the D_{trans} and D_{rot} in this temperature range appear proportional to T/η . However, when the temperature is lowered below $1.2T_g$, the supercooled fragile liquids begin to upset this traditional situation. On one hand, the rotational diffusion rate continues to follow Eq (1b) reasonably well, while on the other hand translational diffusion occurs “too fast” near T_g in comparison with the prediction of Eq (1a). Upon approaching T_g , the discrepancy is often 2 orders of magnitude or more [7, 9, 10]. In other words, for $T_g < T <$

1.2 T_g , there is an apparent “enhancement” of translation relative to rotation. This means that a probe molecule can translate tens of molecular diameters before it rotates 45° [7, 15].

It has been argued [16] that these effects arise from differently averaged measurements due to spatial heterogeneity. Near the glass transition, the dynamics in one region of a supercooled liquid can be orders of magnitude faster than the dynamics in another region only a few nanometers away. The translational and rotational experiments average differently over the heterogeneity. When performing rotational diffusion experiments, molecules in more mobile region (fast region), reorient quickly and are responsible for the fast initial decay in the correlation function, while molecules in less-mobile regions (slow region) are responsible for the long tail of the function [1]. Because the rotational correlation time is the integral of the correlation function, the integral is more sensitive to the long tail compared to the fast initial decay. In contrast, translational diffusion experiments measure the spatial displacement of probe molecules as a function of time. In spatially heterogeneous environments, molecular translation would have the option to move around the slow region rather than enter into it. Then the translational diffusion coefficient would be biased towards the faster portion of the distribution.

Due to the consequences of averaging over different portions of the diffusion distribution, the observed diffusion processes might appear to be misleading. Single molecule methods may give a better answer to this problem. Single molecule orientational microscopy can provide both the rotational and translational motion without having to average over a bulk ensemble, thus seems an ideal tool to the study of the “paradox”.

1-2 Single molecule fluorescence microscopy

The popularity of single molecule experiments has grown tremendously over the past two decades, and has become a powerful technique for exploring the individual nanoscale behavior of molecules in complex local environments. Standard ensemble measurements yield the average value of a parameter for a large number of copies of the molecule of interest. In contrast, single molecule spectroscopy (SMS) completely removes the ensemble averaging, which allows construction of a histogram of the actual distribution of values for an experimental parameter. It is clear that the distribution contains more information than the average value alone. The details of the underlying distribution become crucially important when the system under study is heterogeneous, such as polymers, or glasses. Fortunately, a single molecule can be a local reporter of its “nanoenvironment”. Another advantage of SMS measurements is that, in a time-dependent process, initial synchronization is not required. For example, an enzymatic system may be in one of several catalytic states, and in an ensemble measurement the initial synchronization is required but is quickly lost due to the uncorrelated subsequent dynamics of individual enzymes. However if a single molecule is observed, any one molecule of the ensemble is in only one state at a given time, making different states available for study [17].

One of the most successful approaches in single molecule techniques is single molecule fluorescence microscopy. The two common experimental setups for measuring fluorescence at the single molecule level are confocal microscopy and total internal reflection (TIR) fluorescence microscopy (Fig 1.2) [18]. In confocal microscopy (Fig 1.2,

panel a), a laser is focused to a diffraction-limited spot at the sample plane and excites only a small volume. Emitted fluorescence and back scattered laser light are then collected by the same microscope objective. Residual laser light is filtered out by an emission filter, and fluorescence is focused by the microscope tube lens through a pinhole aperture located at the microscope image plane. The pinhole serves to spatially reject out-of-focal-plane light and gives improved axial resolution. The diameter of the pinhole determines the absolute depth of field for a confocal image. This confocal advantage helps with SMS, since a smaller depth of the sample surrounding the single molecule is allowed to be detected by the detector, the background is reduced and signal-to-noise ratio can be increased. After the pinhole, the emission can be split into multiple channels for acquisition. Also in order to image many molecules, a piezo electronic nano-positioning stage is often used to scan the sample.

TIR microscopy [19] can also be used to observe single molecules with high sensitivity. The two types of TIR microscopy commonly used differ largely by how the excitation light is brought to the sample: through a prism or directly through the objective. Fig 1.2 panel b shows the through prism TIR setup (the through objective TIR will be discussed in detail in next chapter). TIR is generated at a high-index to low-index boundary, mostly at the interface between a glass cover slip and air, and only fluorophores that are sufficiently close to the interface will be excited. The fluorescence is then collected by the microscope objective and is recorded by a CCD camera. The benefit of TIR microscopy over confocal microscopy is that a large area of the sample can be imaged simultaneously, and the drawback of this method is that the CCD camera limits the time resolution.

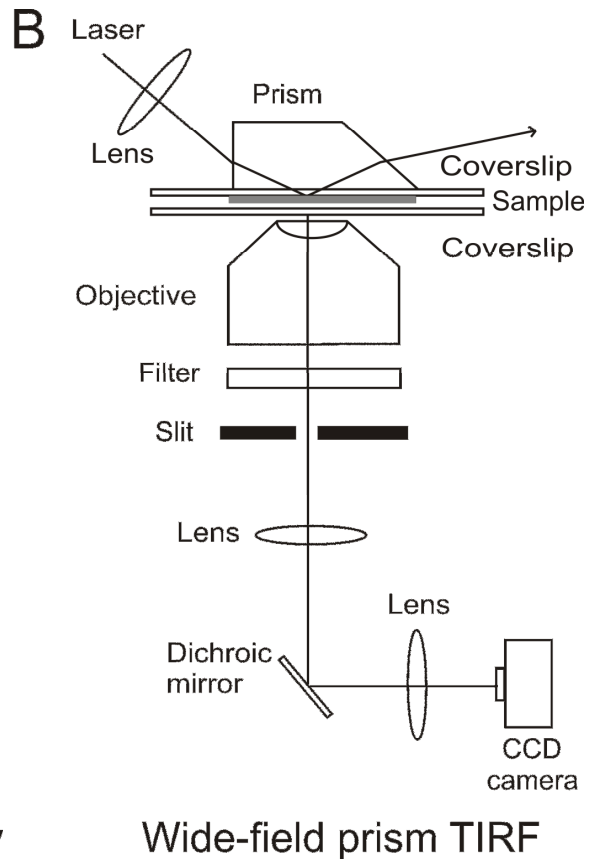
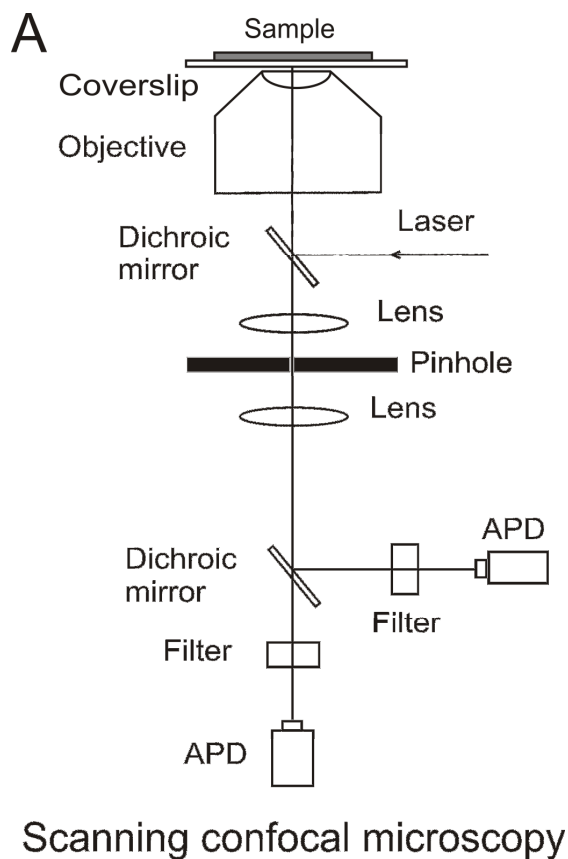


Fig 1.2 Conventional experiment setups used for single molecule fluorescence microscopy (APD: Avalanche photodiode). a) A typical confocal microscope with both the excitation light and emission going through the objective lens. b) A through prism TIR fluorescence microscope where excitation light is reflected through a prism on top of the slide and the emission goes through the objective. Adapted from Ref [18]

Different experimental methods have been developed to study different single molecule behaviors. Fluorescence resonant energy transfer (FRET) [20], for example, works well both in bulk and on the single molecule level for at least qualitatively measuring distances. FRET requires two fluorophores, one as donor and one as acceptor. When a fluorescent dye (donor) is excited by a light source, energy can be transferred to another dye (acceptor), when the donor and acceptor are separated by about 2~8 nm. This distance range is well suited for studying biomolecules. Typically FRET measurements are performed between two different fluorescent dyes where the emission of the donor dye overlaps with the absorption of the acceptor. As the two molecules come closer together, the donor emission intensity decreases while the acceptor emission increases. Since the efficiency of the energy transfer has a strong dependence on the distance between the two molecules, small inter-molecule distance changes can be detected [21]. Since measurements of FRET can provide intra- or intermolecular distance data for proteins and their ligands, it is a sensitive measure of conformational change. So FRET is used to obtain structural maps of complex biological structures, primarily proteins and other macromolecular assemblies such as ribosomes and nucleosomes [22].

Fluorescence imaging with one-nanometer accuracy (FIONA) [22] is a recently developed single molecule technique. A standard TIR microscopy setup is used for these experiments. The basic idea of FIONA is to accurately determine the position of the fluorescent dye molecule in the x, y plane by analyzing the fluorescence image or point spread function and curve-fitting it to a Gaussian function. By locating the position of the dye molecule before and after the molecule of interest has moved, a displacement of as small as ~1.5 nm can be detected.

Both FRET and FIONA measure the lateral displacements of single molecules. To get the whole picture of the single molecules, single molecule polarization microscopy and three-dimensional orientational microscopy allow one to determine the angular orientation of single molecules.

Single molecule polarization techniques are based on the assumption that single fluorescent molecules preferably absorb photons with polarization aligned with the absorption dipole moment of the molecule of interest. Also, emitted photons are polarized along the direction of the emission dipole. One way to extract orientational information is via modulation of the excitation polarization [polarization modulation (PM)] [23]. If the molecule is static or rotating slowly with respect to the integration time, then one can observe a cosine-squared dependence of the fluorescence signal as the polarization of the excitation laser beam is rotated with respect to the molecular transition dipole. An alternative approach to get polarization information involves excitation with circularly polarized light and recording the emission into two orthogonal directions I_S and I_P [24]. The orientation obtained from the above polarization studies is a poor approximation to the 2-dimensional (in-plane) orientation. Many applications, however, require the knowledge of the true in-plane or complete three-dimensional (3D) spatial orientation of molecules and its changes in the course of time. This knowledge could lead to precise studies on the influence of the molecule environment on the molecule physical properties, to investigate external field effects, to measure the orientation factors in energy transfer processes, or to probe spatial heterogeneity in both material and biological systems. In the past, several techniques have been proposed to get the 3D orientation of single molecules [2, 4] [25-30]. Here single molecule orientational microscopy is developed

based on the through objective TIR experiment setup (detailed in Chapter 2). Because molecular emission occurs with a highly anisotropic sine-squared distribution relative to the transition dipole, observed single molecule emission patterns are uniquely characteristic of true 3D orientation. Three dimensional orientations are determined by analyzing the spatial distribution of emission imaged with a CCD camera. Measurement of many such emission patterns as a function of time enables true 3D orientation dynamics of many individual molecules to be followed simultaneously.

CHAPTER 2

EXPERIMENTAL SECTION

2-1 TIR fluorescence microscopy setup

The experimental set up is based on an Olympus IX70 inverted fluorescence microscope (Fig 2.1). The 514 nm beam of an argon ion laser is passed through a quarter wave plate, reflected by a dichroic mirror and focused on the cover glass surface using a 100×, 1.4 NA oil immersion objective (Olympus). The light undergoes total internal reflection at the sample-air interface. There are two advantages of total internal reflection (TIR). First, TIR is a convenient excitation light source because of its ability to generate any polarization light near a surface [31], so molecules can be optically excited regardless their orientation. Second, under TIR, the excitation light undergoes 100% reflection from the interface; the evanescent wave can only illuminate a range of ~100 nm from the interface [31], thus serving as a powerful tool to lower the fluorescence background, which is very important in single molecule studies.

The molecular fluorescence is collected using the same microscope objective, then passes through a 530 nm LP emission filter to reject the excitation source and imaged on to a high sensitivity back illuminated CCD camera (DV887ECS-BV, Andor Technology). Images were typically captured every 100 ms until the dye molecules photo bleach.

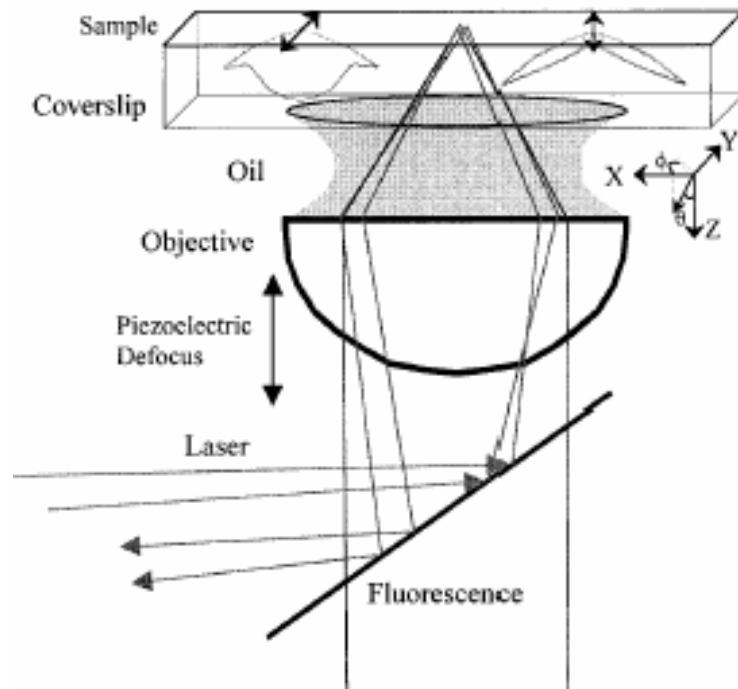


Fig 2.1 TIRFM experimental set up. The excitation light is a 514 nm line of CW argon ion laser. The laser was focused with an achromatic doublet lens (180 mm focal length) and reflected into the microscope objective by a dichroic mirror. The laser goes under TIR at the glass-air interface. The fluorescence emitted from the single molecules was collected by the same objective. [2]

2-2 Polymer thin film near the glass transition temperature

Experiments were carried out on a polymer thin film deposited on cleaned cover glass (BK7). The cover glass was cleaned by first putting into Nochromix with concentrated sulfuric acid solution overnight, then rinsed with DI water and methanol, dried with nitrogen gas, and finally put into UV-Ozone Photo Reactor (PR-100, Ultra-Violet Products, CA) for 2 h before use. The polymer used was poly (isopropyl acrylate) (PIPA), $T_g = 270$ K, molecular weight, $M_w \sim 120,000$ (Scientific Polymer Products, Inc.). PIPA was chosen because of the low glass transition temperature. As discussed in Chapter 1, this research is focused on the polymer in the $T_g < T < 1.2 T_g$ range. However, since the experiments need to be performed on the microscope, the microscope objective's working temperature range (< 60 °C) sets the high temperature limit of the experiments. That required the polymer should have a T_g around 270K, so PIPA was selected. The dye used was Alexa[®]514 (Invitrogen). Alexa was chosen because its fluorescence at higher temperature ($T \sim 60$ °C) is more stable compared with other dyes (data not shown). The chemical structure of PIPA and Alexa are shown in Fig 2.2.

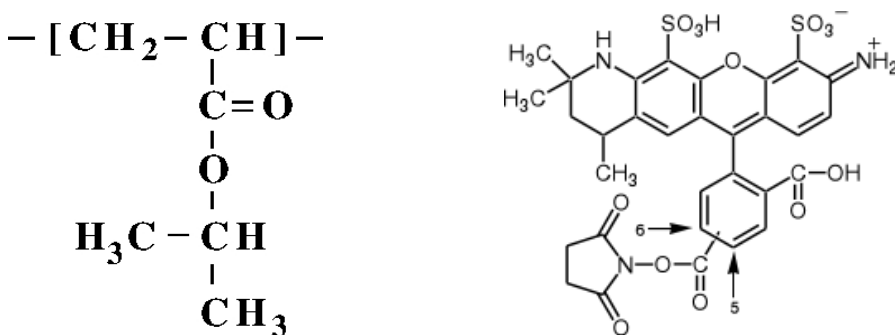


Fig 2.2 Chemical structure of PIPA (left) and Alexa[®]514 (right)

Samples were prepared by spin-casting the polymer and dye in toluene solution (Alexa concentration is about 10^{-9} M) on to the cleaned cover glass. The resulting thin films were annealed at 330K for 10 h to remove residual solvent and to relax influences of the spin coating technique on the polymer conformation. The thickness of the polymer films were determined by a profilometer. The resulting polymer films were approximately 150 nm thick and the dye molecules were well separated. In polymer thin films, the glass transition temperature differs relative to their behavior in the bulk [32-34] because of the confinement effect at the nanometer size scale. The glass transition temperature in thin polymer films has been widely examined [35, 36], and can show different behaviors depending on materials and measurement techniques [37-39]. The results generally show a dependence of the T_g on the film thickness below 50~80 nm [40]. To make it simple, we select the film thickness range of ~150 nm, in this range, the polymer thin film can be treated as bulk [41, 42] and the bulk T_g is used as a reference for both the translational and orientational dynamics.

The sample was mounted onto a home-built microscope stage. Through this stage, vacuum of $\sim 10^{-5}$ torr was applied to reduce the photo bleaching and the dye molecules can remain fluorescent longer. The stage also offers temperature control.

The position and orientation of the single dye molecules is studied by TIR fluorescence microscopy as discussed above. Single molecule tracking was used to study the translational motion at higher temperatures of 40°C, 50°C and 55°C. Emission pattern fitting was used to study the orientational and translational motion at lower temperatures of 5 °C and 10 °C. The time resolution of the experiment is the integration time of the CCD camera, which is 100 ms.

CHAPTER 3

RESULTS AND DISCUSSION

3-1 Emission pattern fitting to determine orientations of single molecules

Single dye molecules are not isotropic light sources. When excited, they emit as anisotropic dipole sources. From this point, emission dipole fluorescence is emitted in a sine squared distribution relative to the dipole axis. Molecules with transition moments aligned along the optic axis emit light only at very high angles relative to the optic axis. In contrast, molecules perpendicular to the optic axis emit light primarily at low angles, directly into the microscope objective. Molecules, therefore, naturally exhibit emission patterns that are uniquely indicative of the molecular orientations [43] [2, 29].

Using a high numerical aperture (NA) objective, the orientation dependent fluorescence patterns can be collected and measured with a CCD detector. The collected single molecule fluorescence emission pattern is accurately modeled by the Kirchoff integral [2]

$$I(x, y, z) = \frac{I_0(\theta, \phi)}{z^2} \left| \int_0^1 J_0 \left(ka\rho \frac{\sqrt{x^2 + y^2}}{z} \right) \exp(-ikopd(\rho)) \cdot \rho \cdot d\rho \right|^2 \quad (1)$$

In this equation, $I(x, y, z)$ is the single molecule fluorescence intensity as a function of detector position, $I(\theta, \phi)$ is the dipole emission pattern defined by polar angles θ and ϕ relative to the interface normal, z is the microscope tube length, k is the wave vector magnitude and is equal to $2\pi/\lambda$, a is the limiting aperture of the imaging system and ρ is the normalized aperture. The $opd(\rho)$ is the optical path difference as function of ρ , and describes the nonideality of the imaging system. While aberrations can amplify emission

pattern anisotropy, single molecule emission dipole orientation information is directly obtainable from both aberrated and unaberrated single molecule images.

The emission pattern data was fit by minimizing a goodness-of-fit parameter (χ^2) while optimizing the angular orientations of the dipole, θ and ϕ . These parametric fits enable accurate 3-D orientation determinations for any single molecule. Fig. 3.1 shows typical CCD images of several dye molecules with different fluorescence emission patterns, indicating different orientations of the molecules.

The left image of Fig 3.1 is an in-focus CCD image. Molecules with emission dipole perpendicular to the sample plane (parallel to the optic axis) are z oriented and appear as a “doughnut” like emission pattern, whereas molecules with the transition dipoles aligned in the x, y plane show a pattern of bright spots. The z oriented molecule emission patterns are spread out over enough pixels to extract orientation information of (θ, ϕ) through computer fitting [2].

However, for the molecules aligned in the x, y plane, their emission patterns are concentrated on fewer pixels than are z -oriented molecules. So there are greater uncertainties in determining the true orientation of these in-plane molecules. This problem is solved by slightly moving objective up ~ 300 nm, to produce slightly out-of-focus images (right image in Fig 3.1).

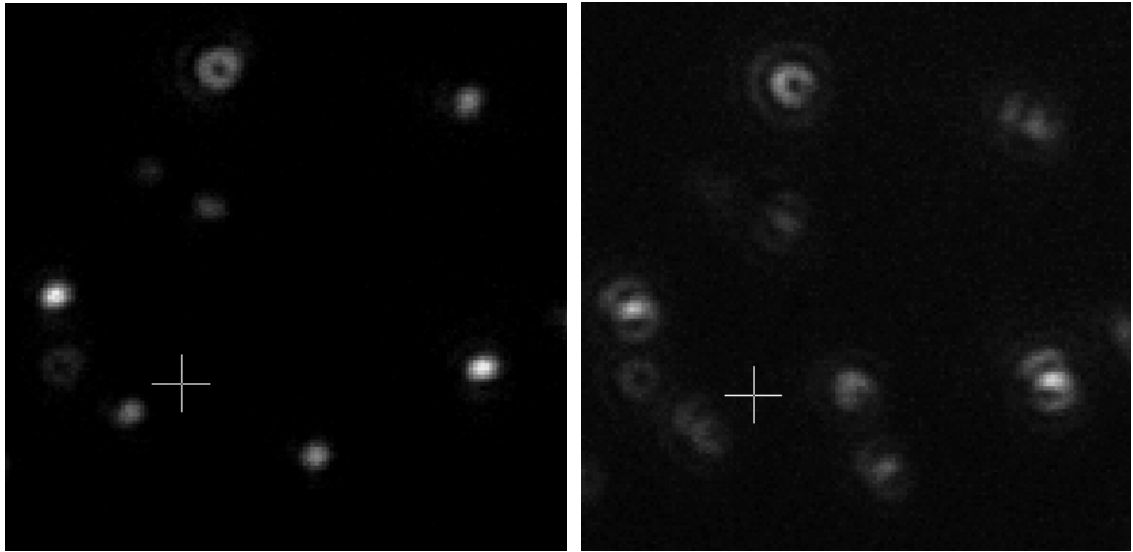


Fig 3.1 Typical CCD images of single molecules. Left: in-focus image. Right: out-of-focus image.

Due to the high angle fluorescence collection efficiency performed by the high NA objective, out-of-focus images result from collecting more of the critical angle emission. The image asymmetry can be seen as “wings”. These wings are perpendicular to the dipole orientation in the x, y plane, and the displacement of the bright feature from the center of the wings gives precise information on both the angle with the optic axis and the position of the molecule. That enables the orientation fitting of the in-plane molecules by our simulations. Fig 3.2 [2] gives examples of emission pattern fitting results.

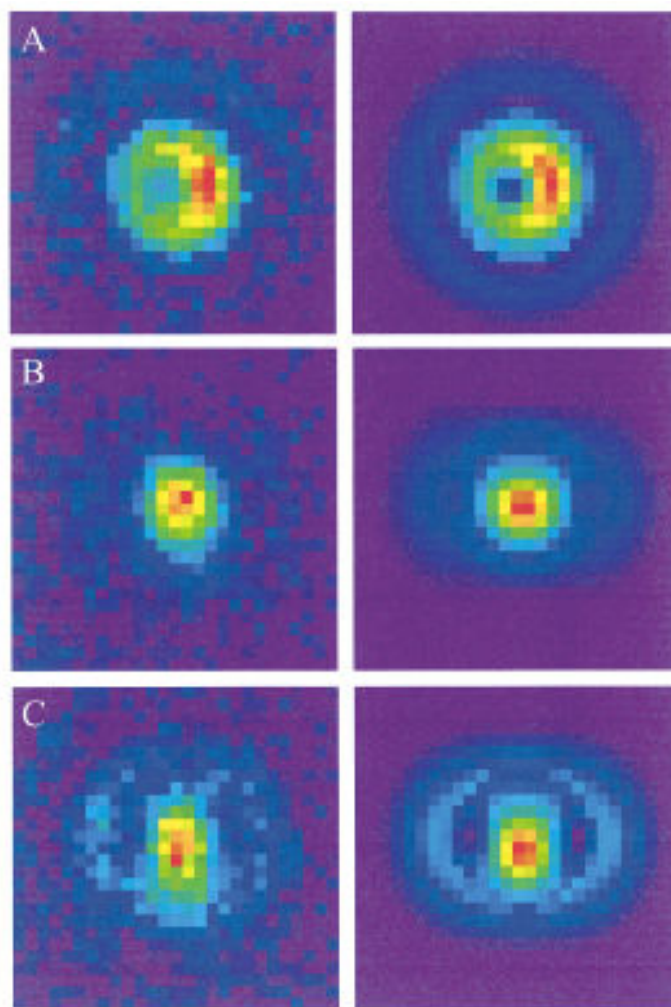


Fig 3.2 Examples of fits of simulated images to experimental emission patterns. [2] The dye used is 1,1'-dioctadecyl-3,3,3',3'-tetramethylindocarbocyanine perchlorate (DiIC18), and the polymer used is poly(methyl methacrylate) (PMMA):
 A) is a z -oriented molecule, the doughnut emission pattern is readily fit, $\theta = 12^\circ$, $\varphi = 6^\circ$.
 B) is an x, y oriented molecule, the emission pattern spread onto fewer pixels and is difficult to find a unique fit. C) is the out-of-focus image of molecule B, the asymmetry of the image indicate the position of the molecule and can be well fitted by the simulation, $\theta = 67^\circ$, $\varphi = 271^\circ$.

Proper emission pattern fitting involves determination of the true position of the single molecule. For any arbitrary orientation, only the out-of-focus emission patterns can provide accurate molecular orientations and positions [2].

A faster way to do the emission pattern fitting is to use the orientational libraries [44]. The idea is, since the emission pattern observed from a given molecular orientation is both unique and characteristic of its true orientation, a library indexed in θ and ϕ can be written for a given set of optical conditions, see Fig 3.3. The library fitting method requires large numbers of images to be simulated first, but for each experimental setup, such libraries only need to be written once. The fitting procedure involves first normalizing the library to the data, then calculating the standard deviation between the experimental image and each image of the library. By searching the whole library, the lowest overall standard deviation gives the molecular orientation.

Similarly, the library fitting method works well with in-focus, z -oriented molecules. In order to fit in-plane molecules, at least one out-of-focus library is required also. If large enough libraries are simulated and searched, library fitting can give orientations with comparable accuracies with parametric fitting results, but much faster. In this respect, library fitting method was used to analyze the orientational and translational dynamics of single molecules in supercooled polymer matrix just above the T_g at 100 ms time resolution.

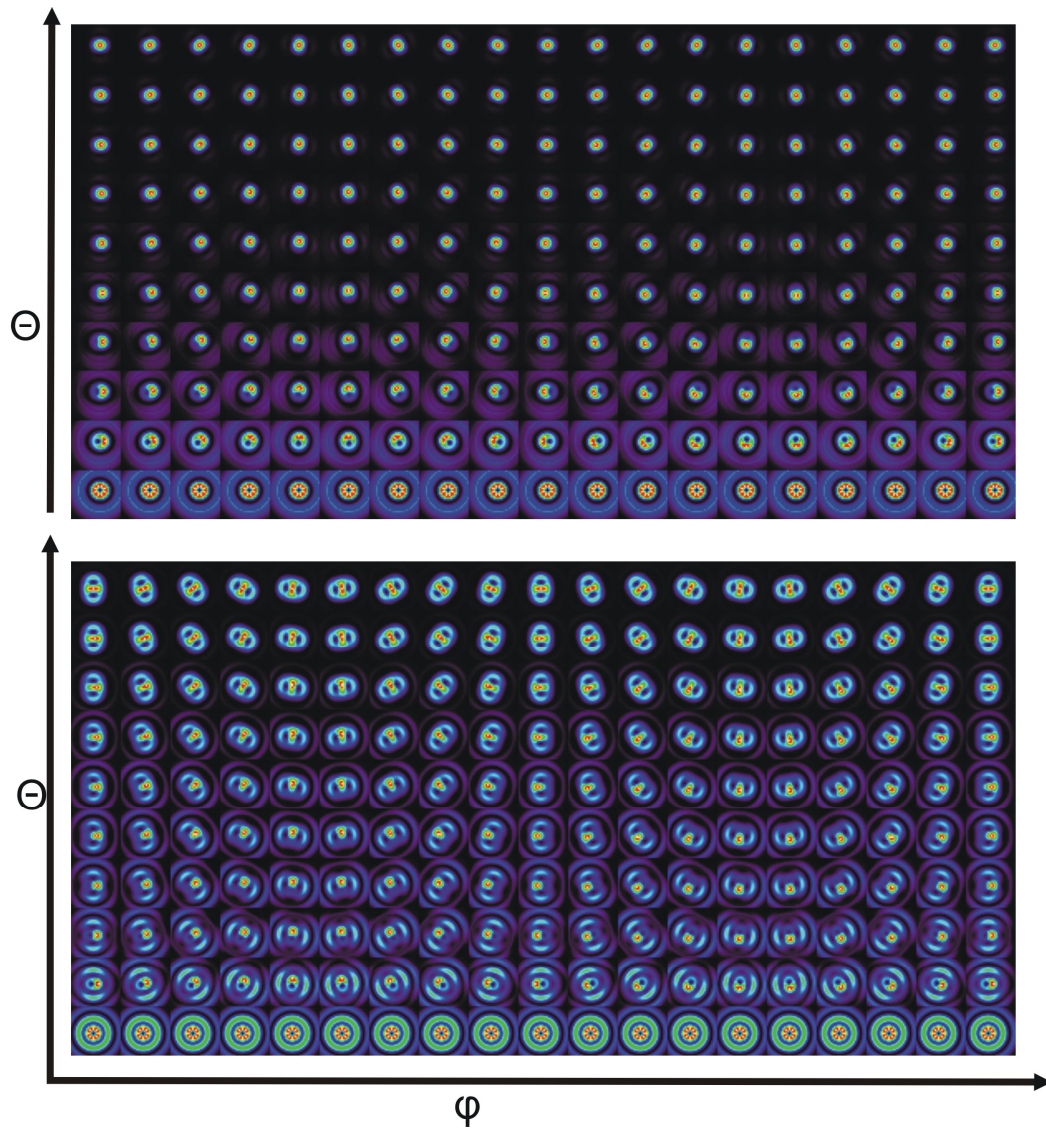


Fig 3.3 Orientational libraries for a specific set of optical conditions. The libraries are indexed in θ and ϕ . The x-axis shows the ϕ changing from $0^\circ \sim 360^\circ$ with 20° increments, and the y-axis is the θ changing from $0^\circ \sim 90^\circ$ with 10° increments. An in-focus orientational library is shown in the top panel and an out-of-focus orientational library shown in the bottom panel.

3-2 Single molecule tracking

To study the translational diffusion of single dye molecules in polymer matrices near T_g , single particle tracking (SPT) was used. In our experiments, the translational diffusion coefficient can be obtained directly from the trajectory of the diffusing particles. At temperatures very close to T_g , $T = 5\text{ }^\circ\text{C}$ and $10\text{ }^\circ\text{C}$, the single molecule rotation is slow enough, so the orientational microscopy method is capable of following the molecular motions and can get both the orientational and translational trajectories. At high temperatures, $T = 40\text{ }^\circ\text{C}$, $50\text{ }^\circ\text{C}$ and $55\text{ }^\circ\text{C}$, where the rotation of the single molecule is too fast, all molecular emission patterns are bright spots devoid of orientational information on the 100 ms timescale. It is also impossible to fit the emission pattern to get the positions. Under this situation, the single molecules are treated as single particles, and use the pixel with maximum intensity as the position of the single molecule to get the translational trajectory. The spatial resolution is the size of the pixel on the CCD camera, with $100\times$ objective and $1.5\times$ microscope expander, it's $\sim 50\text{ nm}$.

3-3 Orientational and translational diffusion results

Orientational diffusion

By employing our 3D orientational single molecule microscopy methods, the orientational changes of many single dye molecules (Alexa) in PIPA thin films can be recorded by CCD camera. After fitting each emission pattern as a function of time, dipolar orientational trajectories $\mu(\theta, \varphi, t)$ can be calculated and used to characterize the dye molecules' dynamics within the polymer matrix. Fig 3.4 illustrates some representative molecular orientational trajectories and the different types of observed single molecule rotational motion in PIPA thin films. As seen in Fig 3.4, ranges in orientational motion vary drastically both in magnitude as well as in rates of orientational change. While all 188 analyzed molecules (104 molecules at 5°C, 84 molecules at 10°C) can be classified as either mobile or immobile, all molecular trajectories exhibited very different dynamics with wide-ranging characteristic time scales. As reporters of local environmental conditions, the different orientational dynamics are likely indicative of the polymer spatial heterogeneity surrounding the probe molecules on the nanometer scale. In the whole set of molecules, nearly half of the molecules (57% at 5°C, 48% at 10°C) remained locked in one preferred orientation. The other half (43% at 5°C, 52% at 10°C) was found to exhibit greater mobility with wide-ranging dynamics that sampled many orientations. These sets of mobile molecules can be further divided into three subset: 1) molecules exhibit fast, nearly free rotation about an average position, illustrated in Fig 3.4 (black trace); molecules that show rotations in only one dimension, either θ or φ (green and pink traces); and molecules that occasionally reorient, changing between a few largely immobile preferred orientations (blue trace).

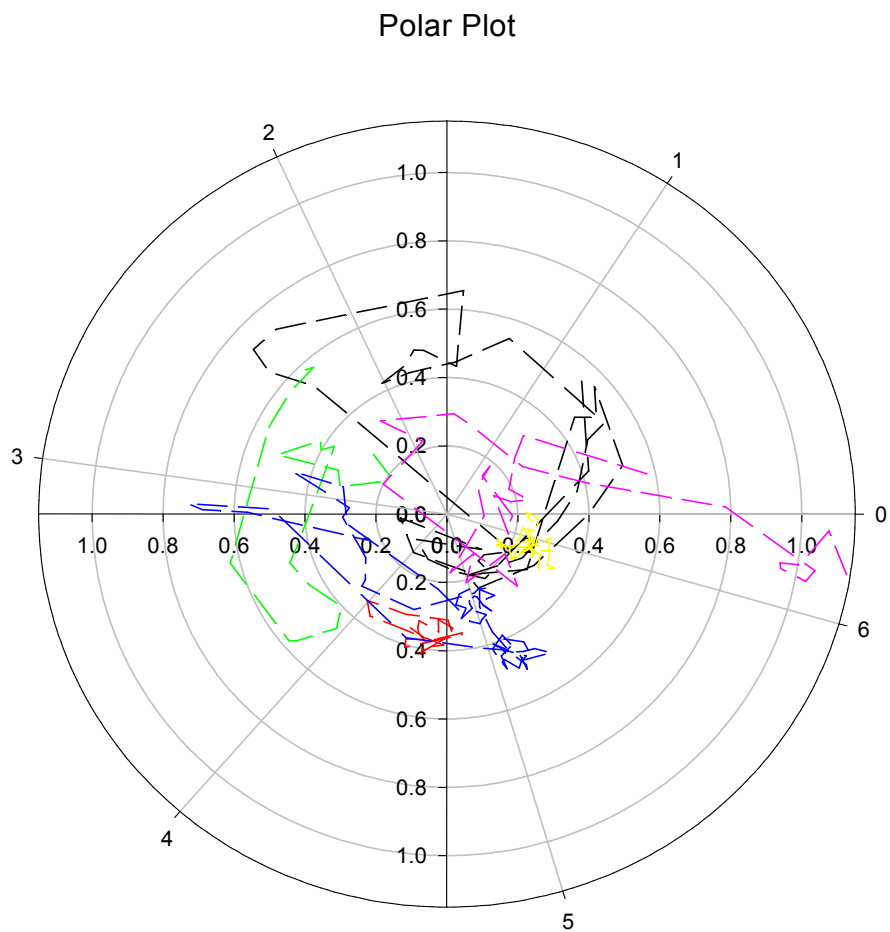


Fig 3.4 Typical orientation trajectories of single dye molecules in PIPA thin films. Different types of single molecule rotational motions are shown in polar coordinates:

- black: nearly free rotation
- green: rotation in φ
- pink: rotation in θ
- blue: a few preferred positions
- red, yellow: one preferred position

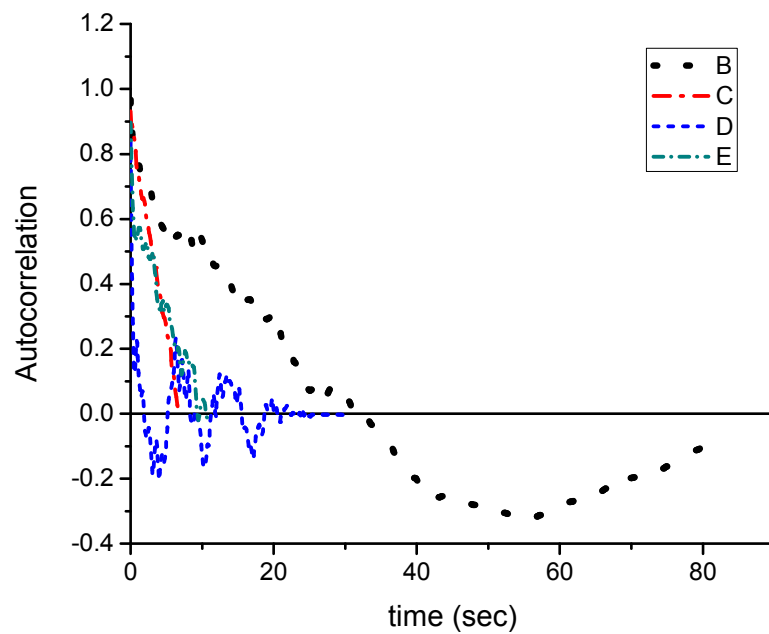


Fig 3.5 Autocorrelation (subtracting the mean orientation) curves of the molecular motions.
 C. E: represent the autocorrelations of molecules remained locked in one preferred orientation.
 B. D: represent the autocorrelations of molecules exhibit greater mobility that sampled many orientations.

The individual molecule orientational dynamics are characterized through the autocorrelation of the dot product of μ_0 and μ_τ , where $\mu_0 = \mu(\theta, \varphi, t_0)$ is the initial dipole orientation and μ_τ is the dipole orientation of all subsequent time steps:

$P_\tau = \langle \mu_0 \cdot \mu_\tau \rangle$. This “memory function” calculates the overlap of the dipole with its original position as a function of delay (τ), thereby providing a full description of the rotational dynamics. In polymer thin films near Tg, the spatial restriction results in a significant overlap of the time-dependent fast dynamics and the time-averaged orientational mean. This 3D single molecule mean dipole orientation can be subtracted from the orientation at each step, and produce the autocorrelation that emphasizes the uncorrelated fast rotational motions characterizing the individual sites [30].

$$P(\tau) = \langle (\mu_\tau - \hat{\mu}) \cdot (\mu_0 - \hat{\mu}) / (\mu_0 - \hat{\mu})^2 \rangle \quad (2)$$

Probe molecules that demonstrate only one preferred orientation did not display interesting rotational dynamics. However, for those probe molecules that sampled many orientations and reoriented among several preferred orientations, oscillatory behavior could be seen clearly in the correlation function. See Fig 3.5. This is the illustration of spatial heterogeneity within the polymer thin films at the experimental timescale. These autocorrelation functions are then fit to an oscillating exponential decay:

$$P(\tau) = A_0 e^{-A_1 \tau} \cdot \cos(A_2 \tau - A_3) \quad (3)$$

Where A_0 , A_1 , A_2 and A_3 are the amplitude, correlation time constant, oscillatory frequency and phase factor, respectively. This equation was fitted to the observed exponential autocorrelation decay, then the characteristic decay time, τ , can be extracted. Because the molecule is rotationally restricted, the autocorrelation decay can be loosely

related to a pseudo rotational diffusion constant that indicates the time scale for losing memory of the initial dipole orientation [30]. The distribution of the pseudo rotational correlation time constant histogram is shown in Fig 3.6. Because probe molecules are rigidly held in polymer films, the molecule must overcome an energy barrier before orientational motion occurs. Each activation energy barrier is unique for the specific probe molecule's local environment. As seen in Fig 3.6, the majority of the molecule population occurs at slow rates (longer correlation time), however, a significant population displays faster rates with shorter correlation time. Although molecules at higher temperature are expected to show faster rotational rates, the experimental data show there is no significant difference between 5 °C and 10 °C. Our experimental limitation comes from the short “live” time before photo bleaching of the Alexa fluorescent dye molecule. Although vacuum was applied on the sample, the dye molecules still inevitably photo bleach in a rather short time under laser excitation (mostly within two minutes). At the same time, our 3D emission pattern fitting method requires enough photons, distributed onto a large area of the CCD, to be collected. This requirement limits studies to slow rotational motions, for which the correlation times are longer than our experimental time scale. Fourkas [4] proposed a method that can determine the 3D orientation of the single molecules at a much faster time resolution. In Chapter 4, our experiment of this 3-detector single molecule orientation determination method is discussed in detail.

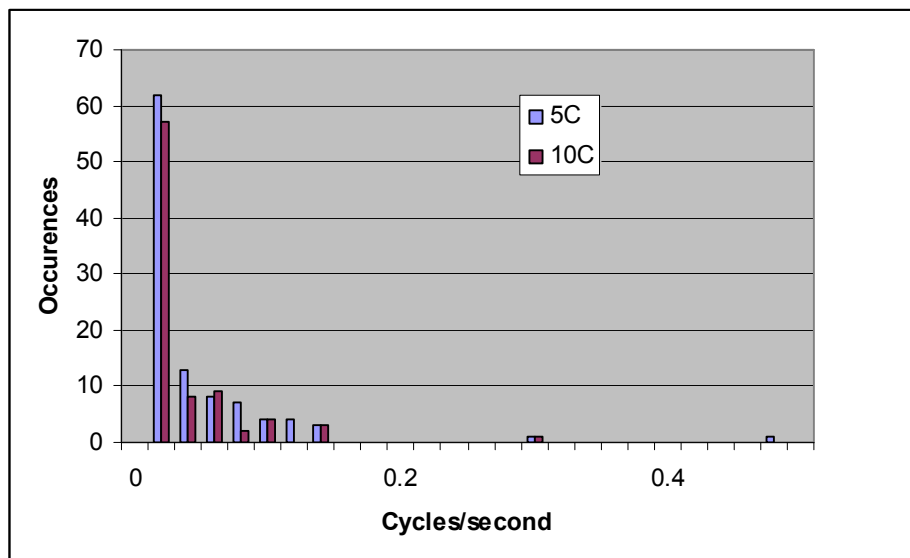


Fig 3.6 Histogram of exponential decay constants for molecules' rotational autocorrelations observed within PIPA films at different temperatures.

Translational diffusion

The simplest mode for a diffusing particle is isotropic random walk, or in other words, Brownian motion. In a random walk, the mean square displacement (MSD) of a diffusing particle $\langle r^2(t) \rangle$ in two dimensions follows a linear dependence with time:

$$\langle r^2(t) \rangle = 4Dt \quad (4)$$

Equation (4), the Einstein equation for a two-dimensional random walk, is the central equation in most diffusion studies. In the microscopic model, the diffusion coefficient D describes the area that the particles explore per unit of time during its random walk.

Starting from a trajectory sampled in time intervals δt , it is easy to calculate the mean square displacement $\langle r^2(t) \rangle$ for every time lag $t = n\delta t$ (n is the number of sample periods between two positions in the trajectory). There are two ways to calculate the MSD for a given time lag δt , by averaging over all pairs of points δt time steps apart, or by averaging over independent pairs of points δt time steps apart [45]. Most of the researchers use the average over all pairs; so does our experiment.

The individual mean square displacements do not necessarily follow a linear dependence with the observation time. In real systems, the diffusion of an individual particle is often influenced by local anisotropies, such as obstacles, regions with a uniform flow, regions with increased viscosity or spatially heterogeneity. These influences are visualized as deviations from the linear behavior in a $\langle r^2(t) \rangle$ versus time plot [3]. For some specific cases, it is possible to derive analytically a mathematical

formula that describes the time dependence of the MSD. A simple collection of such diffusion equations is given below [3]:

$$\langle r^2(t) \rangle = 2nDt \quad \text{random walk in n-dimensions} \quad (5)$$

$$\langle r^2(t) \rangle = 4Dt^\alpha \quad \text{anomalous 2D-diffusion} \quad (6)$$

$$\langle r^2(t) \rangle = 4Dt + (Vt)^2 \quad \text{2D-diffusion with flow} \quad (7)$$

$$\langle r^2(t) \rangle \cong \langle r_c^2 \rangle [1 - A_1 \exp(-4A_2Dt / \langle r_c^2 \rangle)] \quad \text{confined motion} \quad (8)$$

In these equations the MSD as a function of time relate to a diffusion coefficient D.

Equations 5 ~ 8 are plotted in Fig 3.7.

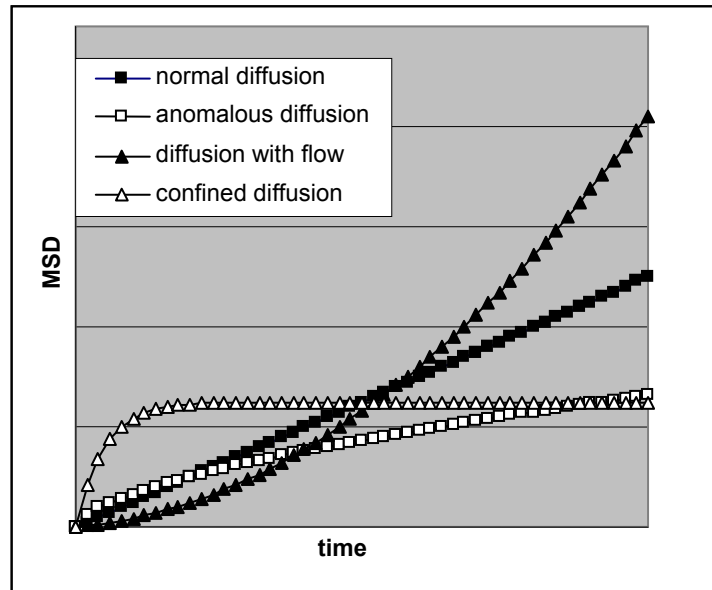


Fig 3.7 Mean square displacements (MSD) as a function of time for different types of diffusion models. The four curves relate to equations (5) ~ (8). The parameters are modified in order to separate different models clearly (normal diffusion: $D=0.125$; anomalous diffusion: $D=0.125$, $\alpha=0.6$; diffusion with flow: $D=0.25$, $V=0.4$; confined diffusion: $D=1.25$, $A_1, A_2=1$)

The normal diffusion gives a straight line through the origin. In the case of anomalous diffusion, in which α is a number between 0 and 1, the curve has a decreasing slope. In the case of diffusion with flow, a constant flow velocity (V) leads to a quadratic increase of MSD with time. In the last case, a molecule diffuses within a confined region. The $\langle r_C^2 \rangle$ corresponds to the effective area of the confinement. The other parameters in equation (8), A_1 and A_2 , relate to the confinement geometry, and are not easily obtained analytically [3].

Using single molecule tracking as explained in Chapter 2, the position of the single dye molecule is determined to be the pixel with the maximum fluorescence intensity on the CCD image. With 100 ms time intervals, Fig 3.8 shows a typical data set, where single molecules show significantly different translational motions. These translational motions can be roughly divided into three kinds of behaviors: first, a large percentage of molecules are moving around within a small area; second, some molecules can travel a long distance in the same thin film; and last, some molecules are locked in one location.

The different translational dynamics shown by the same molecules reside in the same polymer thin films are the direct evidences of spatial heterogeneity. Within the polymers near T_g , the dynamics are not uniform. Fig 3.9 shows a cartoon of spatially heterogeneous dynamics near T_g [1].

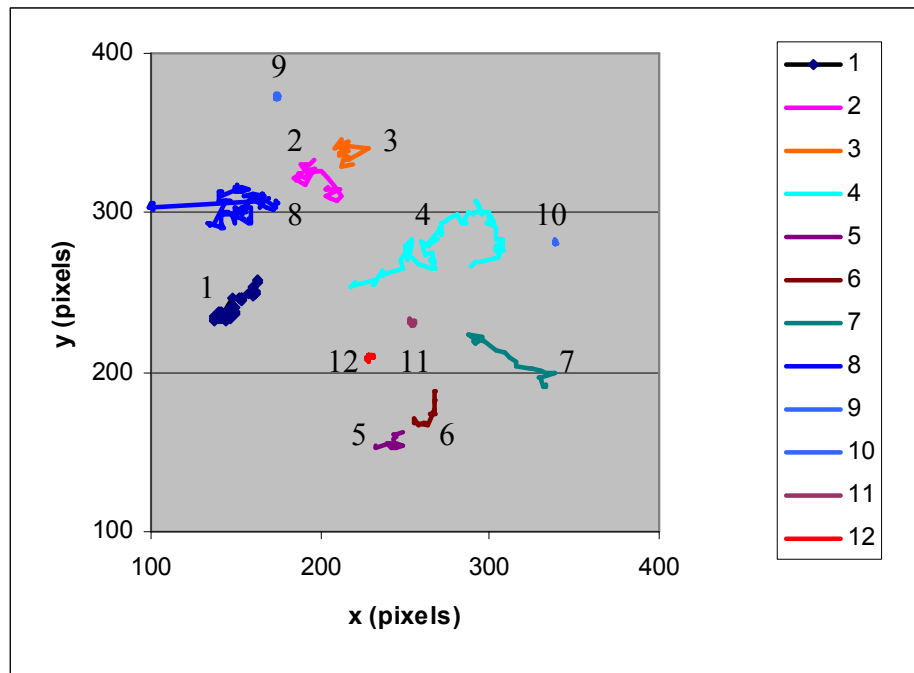


Fig 3.8 A typical data set of single Alexa dye molecule's translational motions in thin PIPA films at $T = 55\text{ }^{\circ}\text{C}$. Molecules show significantly different kinds of motions: 1) molecule 1, 2, 3, 5, 6 are diffusing within a small area; 2) molecule 4, 7 moved a long distance; 3) molecule 9, 10, 11, 12 are clearly immobile molecules; 4) molecule 8's motion is a combination of 2 and 3, traveling a long distance then moving around in a small area.

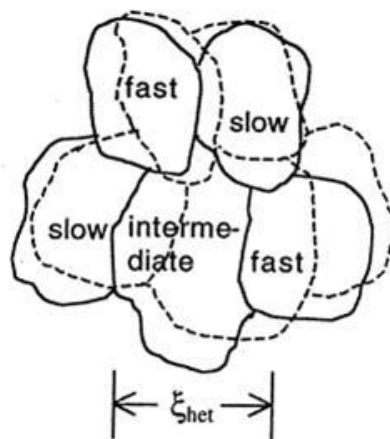


Fig 3.9 Schematic illustration of regions of spatially heterogeneous dynamics of polymer near T_g . These regions are on the order of ξ_{het} in dimension (typically a few nanometers). Reproduced from Ref [1]

In the fast region, with the low viscosity and possibly low energy barrier, molecules (1, 2, 3, 5, and 6 in Fig 3.8) can move around relatively free. In the slow region, molecules are locked in place, and a much higher energy barrier has to be overcome before the molecules (9, 10, 11, and 12 in Fig 3.8) can translate.

At the same time, the different regions are not distinguished by the sharp line as in Fig 3.9; due to the relaxation process, the fast region may become slow region at a later time, and vice versa. That gives the possibility that some molecules (4, 7 in Fig 3.8) can travel from one fast region to another fast region without passing through the slow region.

In order to study the translational diffusion in PIPA thin films near T_g , experiments were performed at different temperatures at the $T_g < T < 1.2 T_g$ range. From the translational trajectories, the mean square displacement (MSD) of each single molecule can be calculated. The different translational dynamics comparison at different temperatures is shown at Fig 3.10.

At higher temperatures, the single molecules move faster compared with motions at lower temperatures. In agreement with the bulk experiment [1, 46], molecules that exhibit increased motions also photo bleach faster. A possible reason is because increased motion enhances the possibility of collision with oxygen molecules, and gets photo bleached. As a result, most molecules with translational motions photo bleach within 10 seconds under laser excitation (0.5 kW/cm^2). At the same time the immobile molecules can stay fluorescent for much longer periods (1 ~ 2 min). Under this experimental limit, the MSD vs. time curves shown in Fig 3.10 can be separated into two different models based on equations (5) ~ (8).

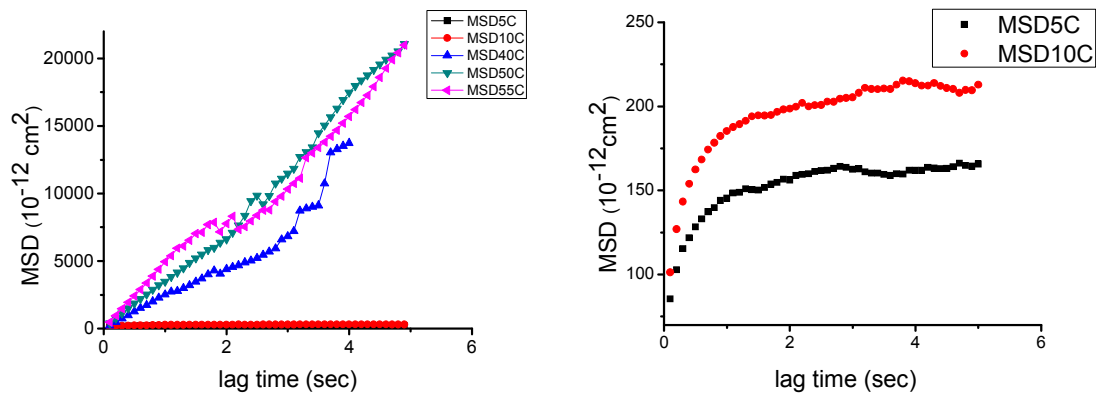


Fig 3.10 Left: Mean square displacement (MSD) comparison of single dye molecules (Alexa) in PIPA thin films at different temperatures.
 Right: detailed curves of MSD vs. time at temperatures 5 °C and 10 °C.

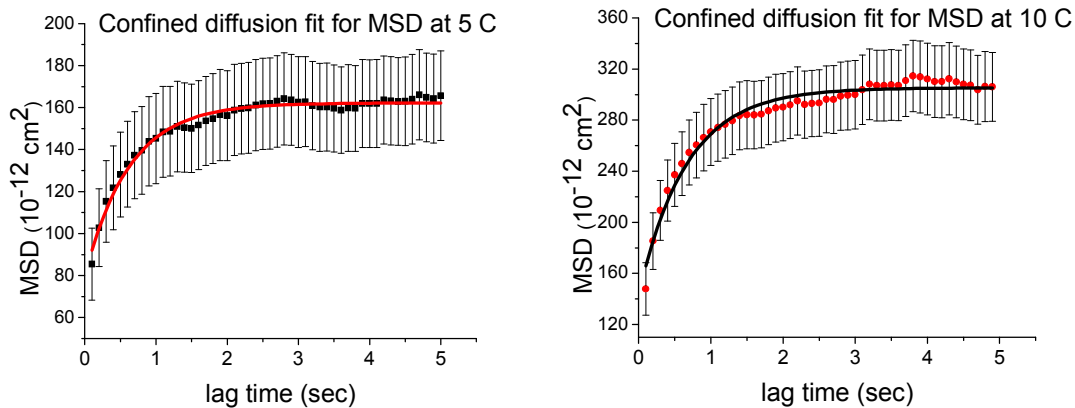


Fig 3.11 Confined diffusion fits for the single dye molecules (Alexa) translational diffusion in PIPA thin films at $T = 5 \text{ }^\circ\text{C}$ and $10 \text{ }^\circ\text{C}$.

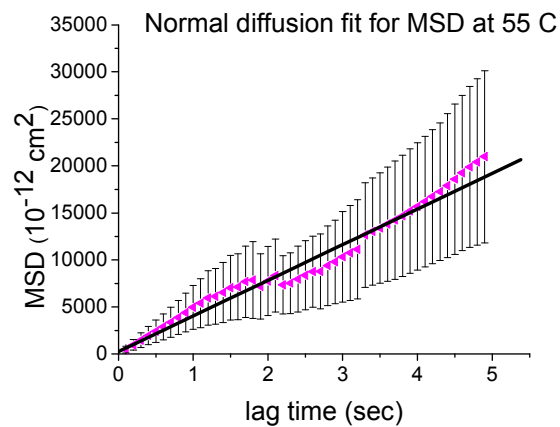
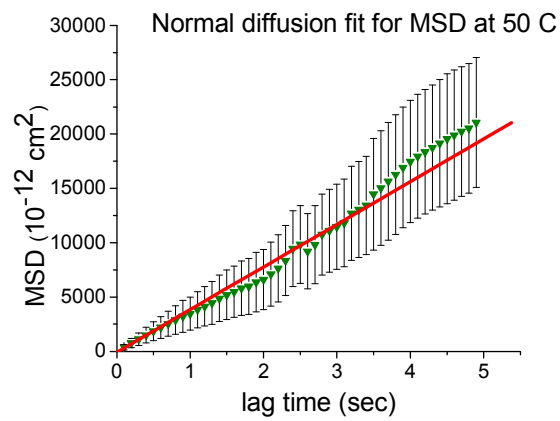
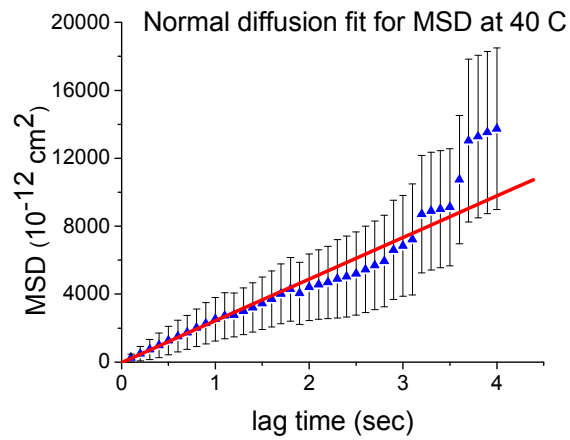


Fig 3.12 Normal diffusion fits for the single dye molecules (Alexa) translational diffusion in PIPA thin films at $T = 40 \text{ }^\circ\text{C}$, $50 \text{ }^\circ\text{C}$, and $55 \text{ }^\circ\text{C}$.

At $T = 5\text{ }^{\circ}\text{C}$ and $10\text{ }^{\circ}\text{C}$ ($T < 1.1\text{ Tg}$) the translational dynamics clearly follow the confined diffusion model. Fig 3.11 shows the fits of the MSD vs. lag time curves to the confined diffusion model Equation (8). The fits yield the effective confinement. They are around $(120\text{nm})^2$ for $5\text{ }^{\circ}\text{C}$, and $(150\text{nm})^2$ for $10\text{ }^{\circ}\text{C}$. The parameters, A_1 and A_2 , relate to the confinement geometry, and assuming the confined areas are circular [47], the calculated translational coefficients D at $5\text{ }^{\circ}\text{C}$ and $10\text{ }^{\circ}\text{C}$ are $25 \times 10^{-12}\text{ cm}^2/\text{s}$ and $31 \times 10^{-12}\text{ cm}^2/\text{s}$, respectively. These confined areas are much bigger than the heterogeneity sizes (several nanometers). Most likely they are the dimensions of the low density area in the polymer matrix. At $T < 1.1\text{ Tg}$, dye molecules can translate slowly within this low density area, possibly from one fast region to another fast region [1], but can not overcome the energy barrier of the confined area.

At $T = 40\text{ }^{\circ}\text{C}$, $50\text{ }^{\circ}\text{C}$ and $55\text{ }^{\circ}\text{C}$ ($T \sim 1.2\text{ Tg}$), the MSD has a linear relationship with time, following the normal diffusion model, see Fig 3.12. That means, for the average of the total analyzed moving molecules, 98 molecules at $55\text{ }^{\circ}\text{C}$, 80 molecules at $50\text{ }^{\circ}\text{C}$ and 76 molecules at $40\text{ }^{\circ}\text{C}$, the molecular behavior follows a random walk within the polymer matrix [48]. However, this is the statistical result of many molecules. For individual molecule's motion, as seen in Fig 3.13, different molecules show different kinds of single molecule's MSD curves with time. So the result is, although on average the MSD obeys the normal diffusion model, the spatial heterogeneity still exist at this temperature ($T = 1.2\text{ Tg}$).

The single probe molecule's translational dynamics within the PIPA thin films are summarized in Table 3.1.

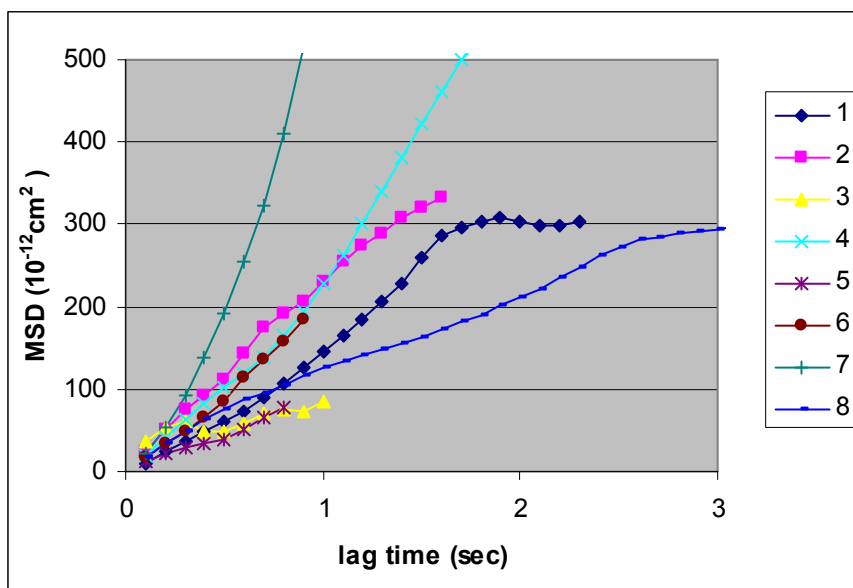


Fig 3.13 Individual molecules MSD vs. time curves. These curves are the 8 moving molecules at 55°C PIPA thin films in Fig 3.9. Although the average diffusion at 55°C follows the normal diffusion model, these 8 molecules show different diffusion behaviors.

Table 3.1 Temperature dependence, population of moving molecules, D and different translational diffusion model in PIPA thin films:

Temperature (K)	% moving molecules	D ($10^{-12}\text{cm}^2/\text{s}$)	Diffusion model
278	N. A.	25	Confined diffusion
283	N. A.	31	Confined diffusion
333	30%	$6.3 \cdot 10^2$	Normal diffusion
353	55%	$9.0 \cdot 10^2$	Normal diffusion
358	60%	$1.2 \cdot 10^3$	Normal diffusion

Conclusion:

Single molecule methods were used to study the polymer dynamics near the glass transition temperature at the single molecule level, beyond ensemble averaging. 3D single molecule orientation determination is used to study the orientational diffusion of probe molecules within PIPA polymer thin films at $T < 1.1 T_g$. Due to the spatial heterogeneity, single probe molecules show dramatically different rotational motions. Autocorrelation analysis shows the rotational diffusion dramatically changes its correlation time within different local environments. The translational diffusion was studied using single molecule tracking. At $T < 1.1 T_g$, the single probe molecule translational diffusion appears to follow the confined flow model. The effective confinement area is larger at higher temperature. At $T > 1.1 T_g$, the results show the probe molecules are more likely at the normal diffusion model. By averaging all the molecules' translational motions, at $T \sim 1.2 T_g$, the MSD analysis yields normal diffusion behavior. That corresponds to the bulk result that there is no heterogeneity at $1.2 T_g$ or higher. However with the single molecule tracking method, the individual molecules show all kinds of diffusion behaviors. That suggests that even at $1.2 T_g$, the spatial heterogeneity still exists.

CHAPTER 4

3-DETECTOR METHODS TO DETERMINE THE 3-D

ORIENTATION OF SINGLE MOLECULE

4-1 Different methods to determine the 3-D orientation of single molecules

During the past decade, single molecule fluorescence spectroscopy has opened a new window to the nanometer scale. Detection of fluorescence from single molecules has become an increasingly important tool for studying microscopic properties in physics, chemistry, molecular biology, and other areas of science, [49] because it gives access to local physical and chemical properties and because it overcomes the loss of information by ensemble averaging. One important dynamic property of single molecules in many systems is molecular orientation. Various photo physical parameters of a single molecule depend on the orientation of the molecule's absorption or emission dipole moment. Fluorophores preferentially absorb photons polarized parallel to the transition dipoles of the molecules [50]. These dipoles have well-defined orientations with respect to the molecular axis. Similarly, emission also occurs with light polarized along this axis.

Various methods have been developed to determine orientations of single molecules [2, 25-28, 51-53]. They can be separated roughly into two kinds of methods: two-dimensional [51, 52] and three-dimensional [2, 25-28, 53]. The two-dimensional method measures the fluorescence anisotropy of single molecules. It is used in many applications in which it is sufficient to measure only the component of molecular orientation within the plane perpendicular to the optical axis of the microscope. This works best for low numerical aperture (NA) collection, but has significant problems at high NA, which are often overlooked.

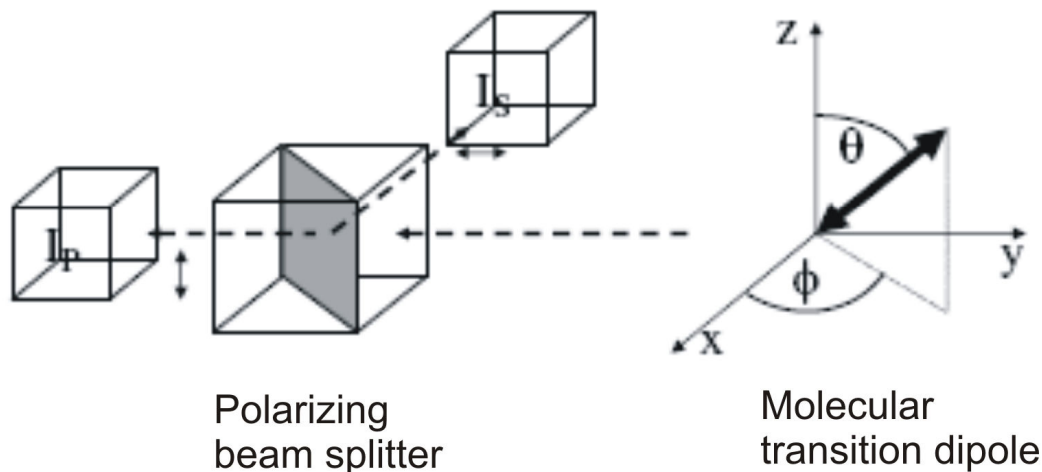


Fig 4.1 Schematic experimental setup: the polarization of light emitted by a single molecule depends on the orientation of the transition dipoles with respect to the detection system. The two orthogonally polarized components of the signal are separated by a polarizing cube beam splitter.

A schematic experimental setup of a typical two-dimensional orientational measurement is shown in Fig 4.1 [50]. In 2D experiment, a circularly-polarized light is normally used for excitation. The double arrow in Fig 4.1 represents the transition dipole of the single molecule. Then the fluorescence from the single molecules passes the polarization beam splitter, separated into two orthogonal polarizations. The ratio of counts at the two polarizations (I_S and I_P) is then used to approximate the in-plane orientation of the fluorescence transition dipole. The reduced linear dichroism d can be calculated from I_P and I_S . This value d is frequently used to study the molecular rotational dynamics.

$$d = \frac{(I_P - I_S)}{(I_P + I_S)} \quad (1)$$

There is a disadvantage of two-dimensional method. Because the molecular emission is dipolar in nature, when high NA objective is used to collect the fluorescence, the dipolar nature out-of-plane emission contribution to the fluorescence signal have to be considered. The standard two-dimensional orientational analysis is valid only in the limit

that emission is collected though an infinitely small cone angle (zero numerical aperture). Using finite numerical aperture objectives will influence the orientation determination, but is incorrectly ignored in most analyses.

True three-dimensional methods can determine the full three-dimensional orientation of single molecules. It can be further divided into those in which the spatial intensity pattern of the emission is analyzed [2, 25-27, 29, 30] and those in which the polarization of the emission is analyzed [4, 28, 53]. Both techniques are capable of yielding enough information to determine the complete three-dimensional orientation of the single molecule. The emission pattern fitting method, which was already discussed in detail in Chapters 2 and 3, require collection of a considerable number of photons, followed by complex and time-consuming image analysis. As a result, the fastest time scale it can access is around 100 ms.

In contrast, Fourkas [4] proposed a method where the signal of three detectors can be exploited to obtain the full orientation information without fitting. Consider a molecule embedded in a medium of index of refraction n (Fig 4.2) that is observed using an objective with a numerical aperture of NA, so the light from the molecule is collected over a cone angle of $\alpha = \sin^{-1}(NA/n)$. The orientation of the fluorescence transition dipole (\mathbf{D}) with respect to the z axis is described with the spherical-coordinate angles Θ and Φ , $D = \sin \Theta \cos \Phi \hat{i} + \sin \Theta \sin \Phi \hat{j} + \cos \Theta \hat{k}$ (Fig 4.2). Similarly, the propagation vector (\mathbf{P}) of an individual ray of fluorescence is described by the coordinates θ and ϕ , $P = \sin \theta \cos \phi \hat{i} + \sin \theta \sin \phi \hat{j} + \cos \theta \hat{k}$ (Fig 4.2).

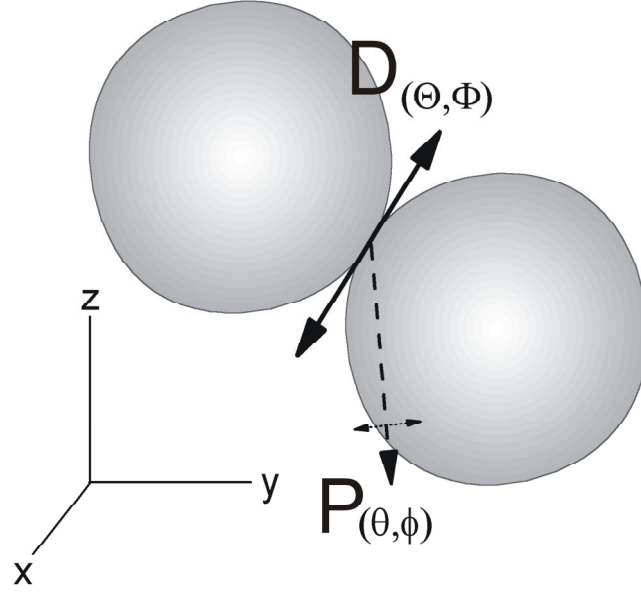


Fig 4.2 Schematic figure of a transition dipole orientation. From Ref [4]. The double arrow represent the transition dipole \mathbf{D} , with spherical-coordinate angles (Θ, Φ) ; the dashed arrow represents the propagation vector \mathbf{P} of an individual ray of fluorescence, with coordinates (θ, ϕ) ; the x, y and z coordinates represent the microscope coordinates with the z axis passing through the center of the objective.

The electric-field polarization vector of a given ray of any direction, $\boldsymbol{\eta}$, can be calculated by $\boldsymbol{\eta} = \mathbf{P} \times \mathbf{D} \times \mathbf{P}$. Evaluation of this cross product [4] leads to

$$\boldsymbol{\eta} = \begin{bmatrix} (\cos^2 \theta + \sin^2 \theta \sin^2 \phi) \sin \Theta \cos \Phi - \sin \theta \cos \theta \cos \phi \cos \Theta - \sin^2 \theta \sin \phi \cos \phi \sin \Theta \sin \Phi \\ -\sin^2 \theta \sin \phi \cos \phi \sin \Theta \cos \Phi - \sin \theta \cos \theta \cos \phi \cos \Theta + (\cos^2 \theta + \sin^2 \theta \cos^2 \phi) \sin \Theta \sin \Phi \\ -\sin \theta \cos \theta \cos \phi \sin \Theta \cos \Phi + \sin^2 \Theta \cos \Theta - \sin \theta \cos \theta \sin \phi \sin \Theta \sin \Phi \end{bmatrix} \quad (2)$$

Where the three rows of the matrix correspond to the components along the x, y and z axis, respectively.

From Equation (2), the polarization vector of light at any position on the objective for a given orientation of the molecule can be calculated. In the experiment, the

microscope objective causes all of the rays that it collects to propagate along the z axis.

Rotating each propagation ray accordingly [4] leads to

$$\boldsymbol{\eta} = \begin{bmatrix} (\sin^2 \phi + \cos \theta \cos^2 \phi) \sin \Theta \cos \Phi - \sin \theta \cos \phi \cos \Theta + (\cos \theta - 1) \sin \phi \cos \phi \sin \Theta \sin \Phi \\ (\cos \theta - 1) \sin \phi \cos \phi \sin \Theta \cos \Phi - \sin \theta \sin \phi \cos \Theta + (\cos^2 \phi + \cos \theta \sin^2 \phi) \sin \Theta \sin \Phi \\ 0 \end{bmatrix} \quad (3)$$

After passing through a polarizer in the x - y plane that transmits light of a polarization that makes an angle γ with the x axis, then the magnitude of the electric field that makes it through the polarizer between times t and $t + \tau$ is given by [4]

$$\begin{aligned} \frac{E(\theta, \phi, \Theta, \Phi)}{E_{tot}(t, t + \tau)} = & \left((\sin^2 \phi + \cos \theta \cos^2 \phi) \cos \gamma + \sin \phi \cos \phi (\cos \theta - 1) \sin \gamma \right) \sin \Theta \cos \Phi \\ & - \sin \theta (\cos \phi \cos \gamma + \sin \phi \sin \gamma) \cos \Theta \\ & + \left(\sin \phi \cos \phi (\cos \theta - 1) \cos \gamma + (\cos^2 \phi + \cos \theta \sin^2 \phi) \sin \gamma \right) \sin \Theta \sin \Phi \end{aligned} \quad (4)$$

where $E_{tot}(t, t + \tau)$ is the total electric field amplitude generated by the molecule in this time period. The intensity of this ray after passing through the polarizer is given by the square of equation (4). This is the intensity at a detector placed after the polarizer at azimuthal angles of 0° , 45° , 90° and 135° , integrated over ϕ from 0 to 2π and over θ from 0 to α yields [4]

$$I_0(\Theta, \Phi) = I_{tot}(t, t + \tau) (A + B \sin^2 \Theta + C \sin^2 \Theta \cos 2\Phi) \quad (5a)$$

$$I_{45}(\Theta, \Phi) = I_{tot}(t, t + \tau) (A + B \sin^2 \Theta + C \sin^2 \Theta \sin 2\Phi) \quad (5b)$$

$$I_{90}(\Theta, \Phi) = I_{tot}(t, t + \tau) \left(A + B \sin^2 \Theta - C \sin^2 \Theta \cos 2\Phi \right) \quad (5c)$$

$$I_{135}(\Theta, \Phi) = I_{tot}(t, t + \tau) \left(A + B \sin^2 \Theta + C \sin^2 \Theta \sin 2\Phi \right) \quad (5d)$$

where

$$A = \frac{1}{6} - \frac{1}{4} \cos \alpha + \frac{1}{12} \cos^3 \alpha \quad (6a)$$

$$B = \frac{1}{8} \cos \alpha - \frac{1}{8} \cos^3 \alpha \quad (6b)$$

$$C = \frac{7}{48} - \frac{1}{16} \cos \alpha - \frac{1}{16} \cos^2 \alpha - \frac{1}{48} \cos^3 \alpha \quad (6c)$$

The three unknown parameters in equations (5), Θ , Φ and $I_{tot}(t, t + \tau)$ can be determined from any three of these intensities. Following Fourkas' predictions, we use 0° , 45° and 90° to get

$$\Phi = \frac{1}{2} \tan^{-1} \left\{ \left[I_{45}(\Theta, \Phi) - \frac{I_0(\Theta, \Phi) + I_{90}(\Theta, \Phi)}{2} \right] / \left[\frac{I_0(\Theta, \Phi) - I_{90}(\Theta, \Phi)}{2} \right] \right\} \quad (7)$$

$$I_{tot}(t, t + \tau) = \frac{1}{2A} \left[\left(1 - \frac{B}{C \cos 2\Phi} \right) I_0 + \left(1 + \frac{B}{C \cos 2\Phi} \right) I_{90} \right] \quad (8)$$

$$\Theta = \sin^{-1} \left\{ \left[\frac{I_0(\Theta, \Phi) - I_{90}(\Theta, \Phi)}{2I_{tot}(t, t + \tau)C \cos 2\Phi} \right]^{1/2} \right\} \quad (9)$$

The orientation determination from equations (7) and (9) doesn't require obtaining a spatial intensity pattern, but just the collecting of enough photons at the three detectors. And the calculation of orientation is simple and fast, not needing to go through image analysis.

4-2 3-detector method experiment set up

In this section, the two methods, three-dimensional emission pattern fitting and the three-detector polarization method, are compared by the following experiment. The outlined experimental setup is shown in Fig 4.3. Similar to the previous experimental setup in Chapter 2, a 514 nm laser line, passes through a 1.4 NA 100× oil-immersion objective, and is used to excite the sample. Then the fluorescence emitted from the single molecule is collected by the same objective. To do the emission pattern fitting, as in Chapter 2, the fluorescence was directed to a CCD camera and the images were recorded and analyzed by our emission pattern fitting programs.

The second part of the experimental setup was for the three-detector measurement. It is basically a confocal microscope setup combined with TIR illumination. First, the fluorescence collected by the microscope objective was aligned to go through a 150 μm pinhole. This enabled us to only collect the fluorescence from a 1.5 μm diameter area of the sample plane, which means that for well-dispersed fluorophores, the emission from only one molecule can be recorded at a time. Second, the focused fluorescence was collimated by an achromatic doublet lens (25 mm focal length) and separated by 50/50 beam splitter. After that, one beam goes through a polarizing cube beam splitter (Newport), and further divided into two beams, the horizontal (0°) and vertical components (90°). These two signals were recorded by two photomultiplier modules (PMT H7422-40, Hamamatsu Photonics, Japan). The other fluorescence light beam goes through the second polarizing cube beam splitter, which was rotated to 45° with respect to the optic table to serve as the 45° polarizer. The fluorescence light then was focused by another achromatic doublet lens (25 mm focal length) onto a single photon-counting module (SPCM-AQR-WX, Perkin-Elmer, Fremont, CA). Finally, all the three channels of signals were directed to the 4 channel Time-Correlated Single Photon

Counting (TCSPC) router (HRT-41, Photonic Solutions Plc, UK), connected to the Becker-Hickl Board (SPC-630, Becker & Hickl GmbH, Germany). The computer controlled program records the time traces of photons in each of the three channels at 50 ns intervals. Then the time traces of the three detectors can be used to calculate the orientation of the single molecule using Equations (7) and (9).

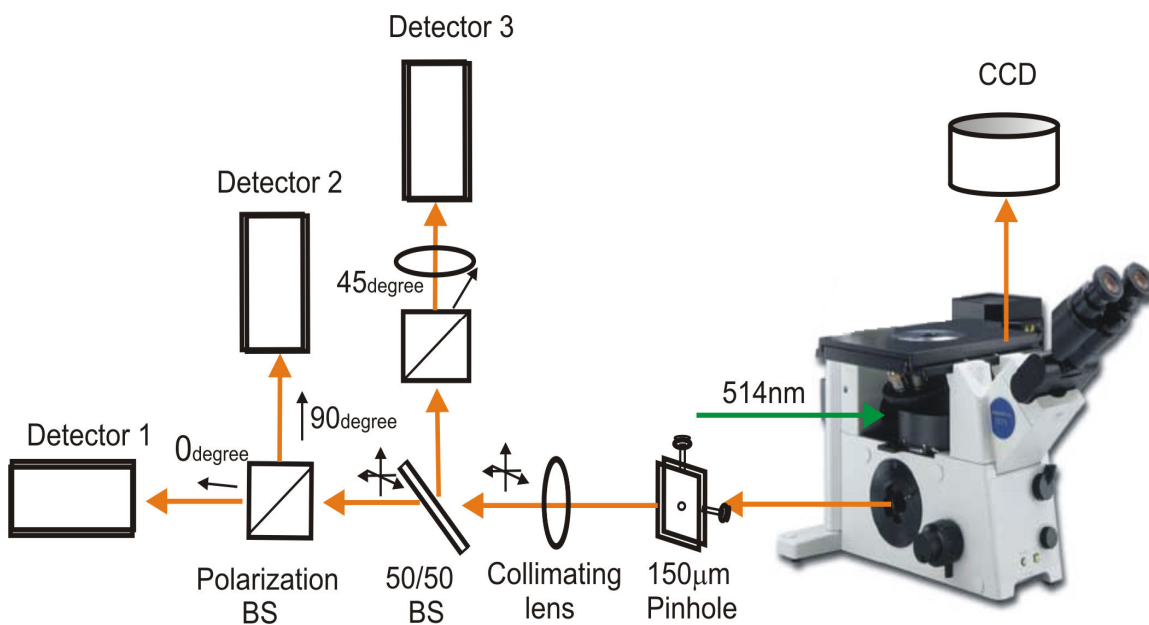


Fig 4.3 Experiment setup for comparing 3D methods of determining the orientation of single molecules. The excitation light is a 514 nm line of a CW argon ion laser focus on the sample through a 1.4 NA 100× oil-immersion objective, and then it undergoes TIR at the sample-air interface. The fluorescence emitted from the single molecule is collected by the same objective, passes the dichroic mirror, and is further filtered by a dielectric long pass filter blocking scattered and back-reflected laser light. For emission pattern fitting, the fluorescence is directed to and recorded by the CCD camera. For the three-detector method, the fluorescence comes out from the side port, goes through all the alignment, and then recorded by the three detectors.

4-3 Results and discussion

The three-detector method uses three different detectors to measure the fluorescence intensities passed through polarizers with different angles. To correct for the different detection efficiencies, fluorescent latex beads (20 nm, Molecular Probes) were used to act as an isotropic emission source, in other words, the fluorescence emitted from these fluorescent beads are the same at all different polarizations. Therefore, after different angles of polarizers, the three detectors should get the same fluorescent intensities. After compensating for the detectors' efficiencies, the fluorescence intensities were used to calculate the orientation of the single molecules.

The sample used to do the single molecule experiment was prepared by spin casting a polymer film from a solution of poly(methylmethacrylate) (PMMA, MW=350,000) and 1,1'-dioctadecyl-3,3,3',3'-tetramethylindocarbocyanine perchlorate (DiIC₁₈, Invitrogen) in toluene onto a microscope cover glass. The final concentration of the solution is: 10⁻⁴ M for PMMA, 10⁻¹³ M for DiIC₁₈. The resulting polymer film was approximately 100 nm thick and the dye molecules were well-separated. The glass transition temperature (T_g) of PMMA is 120 °C, and the experiment was performed at room temperature, well below T_g of the PMMA. As discussed in Chapter 3, the dynamics, both translational and orientational, are so slow that the dye molecules can be treated as immobilized. Also former experiment results shows that the DiIC₁₈, in this PMMA thin film, and this temperature range, 97% were completely immobile on our experimental timescales (several minutes). Under this assumption, the experimental procedure was to first move a single dye molecule to the confocal position, where the emitted fluorescence can pass the 150 μm pinhole. A scanning stage (NSOM TOPAZ Electronic Controller, Nanonics Imaging Ltd.) was used to hold the cover glass, and position the single dye molecule to the confocal position. The defocused CCD image was then taken for the emission pattern fit. After that, the molecule was re-focused and the

fluorescence directed to the microscope side port to make the three-detector measurement.

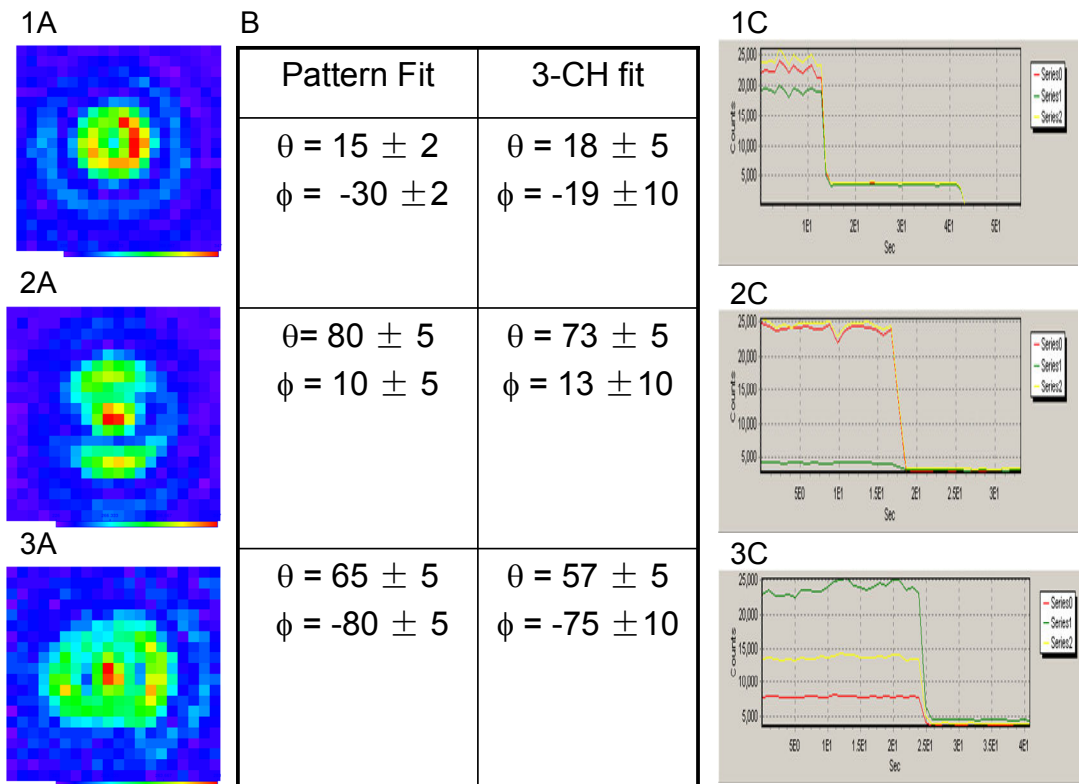


Fig 4.4 Typical data from pattern fit method and three-detector method. 1A, 2A, 3A: single dye molecule fluorescence emission pattern from CCD camera, integration time is 100ms. 1C, 2C, 3C: single dye molecule fluorescence intensities traces detected from different detectors after 0°, 45°, 90° polarizers, integration time used is also 100 ms. B: single molecule orientation determined by the two methods.

Since the single molecule is immobile, the two methods should give the same orientation results. Fig 4.4 shows the typical data from the two methods studying the same molecule.

The experimental result shows that the pattern fit method and 3-detector method gave comparable orientation for the same single molecule. In Fig 4.4, the CCD image of molecule A is a donut pattern, an out-of-plane molecule ($\theta=15^\circ$), means the transition dipole of molecule A is nearly aligned with the z axis, perpendicular to the sample plane. When projected to the x, y plane, there is little difference among 0° , 45° and 90° polarizations. Accordingly the three fluorescence intensities detected by the three detectors are very close. Molecule B and C are in-plane molecules. The in plane angle of B is 10° , so in the 3-detector data, the 0° channel intensity is much higher, and the 90° channel intensity is nearly zero. Similar results were obtained for molecule C ($\varphi=-80^\circ$), the 90° channel intensity is much higher than 0° channel.

One of the advantages of the 3-detector method is it can go faster than the pattern fitting method. In pattern fitting, the fastest practical time resolution is ~ 100 ms. By using the 3-detector method, we can determine the orientation of the single molecule at ~ 10 ms time resolution (Fig 4.5). The accuracy of the orientation calculated from the 3-detector method depends on how many photons are detected in the specific time range. The shorter the integral time, the more fluctuation will arise in the calculated orientation. The 10 ms data has a higher error range compared to the 1s integral time. However, even at 10 ms, it still gives a reasonable orientation result.

The accuracy of the 3-detector method is a little bit lower than emission pattern fit method. The emission pattern fit can give $\sim 2^\circ$ accuracy for out-of-plane molecules [2], and $\sim 5^\circ$ for in-plane molecules.

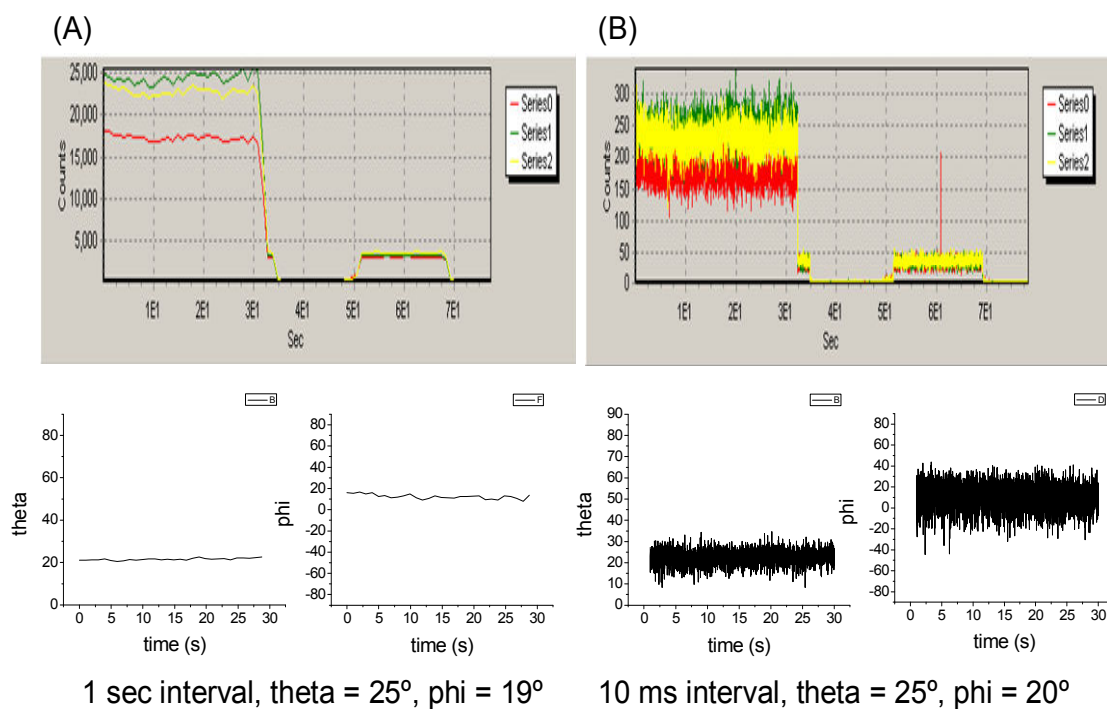


Fig 4.5 The 3-detector data at different time resolution. Above is a set of 3-detector data from the same single molecule. (A): the integral time is 1 s, orientation calculated is $\theta=22^\circ \pm 2^\circ$, $\phi=15^\circ \pm 2^\circ$. (B): the integral time is 10 ms, orientation calculated is $\theta=25^\circ \pm 6^\circ$, $\phi=20^\circ \pm 10^\circ$.

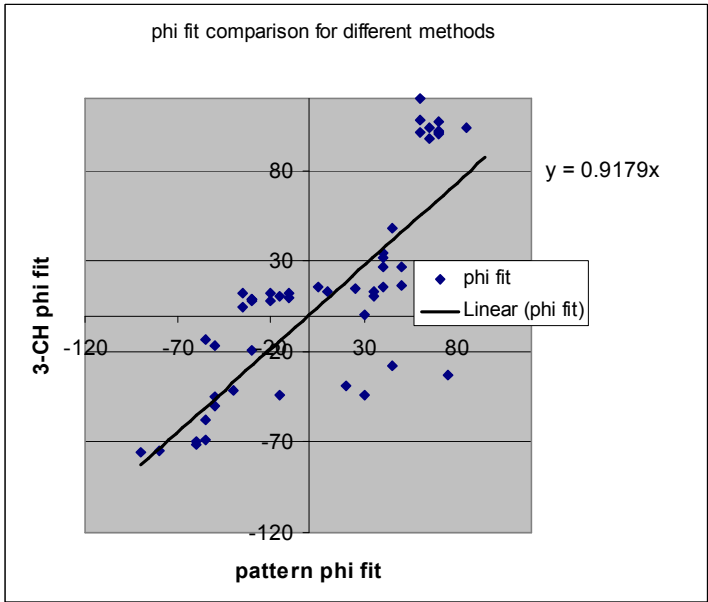
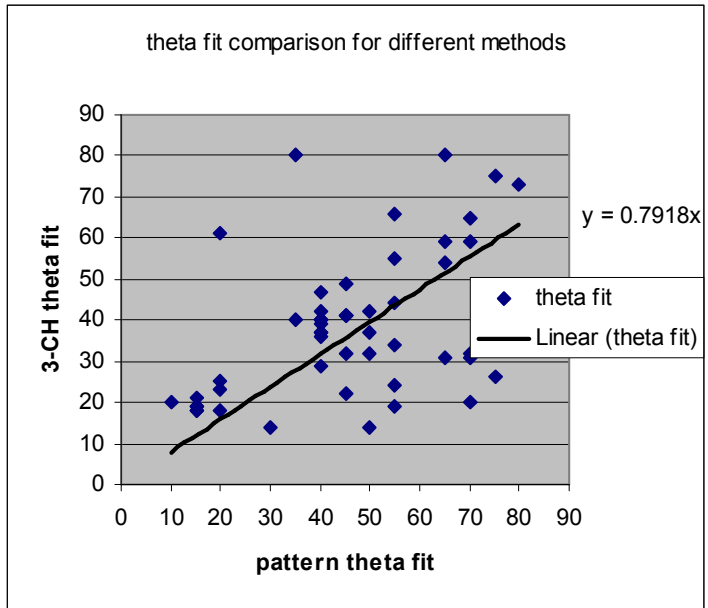


Fig 4.6 Orientation fit result comparison for different methods.
 Top figure: the theta fit comparison.
 Bottom figure: the phi fit comparison.

Fig 4.6 is the comparison of the fitting results from these two different methods. It shows that for fitting results of θ , the average error range is $\sim 10^\circ$, and for φ , it falls in the range of $\sim 20^\circ$. In Fig 4.6, for some molecules, there is a large discrepancy between the 3-detector fit and emission pattern fit. The discrepancy is not coming from the error, most likely coming from the rotation of the molecule during the experimental measurements. As stated earlier, the molecule's emission pattern was recorded first; the 3-detector data were recorded after. Since most of the molecules are immobile, so the two methods will give compatible orientation results. However, some molecules do rotate during that time range, and the rotation causes the disagreement between the fitting results from these two methods. Also it has to be noticed that there is a two fold degeneracy of the determined orientation due to the symmetry of the dipole and the 3-detector experimental setup, resulting in a range for θ is from 0° to 90° , and φ from -90° to 90° .

From Fig 4.5, we can see that the 3-detector method fitting give a rather close fit for in-plane molecules. There are two reasons. First, due to the experiment setup, the microscope objective can collect the fluorescence light at a cone angle of α , if the molecule is aligned along the z axis, only part of the fluorescence can be collected. By summing the intensities seen at 0° , 45° and 90° , we find that the total signal from a molecule aligned with the z axis is approximately half of that for a molecule in the x, y plane. The more photons it can collect, the more accurate the fitting result can be. Second, the azimuthal angle φ is a strong function of θ . Calculation shows that for a molecule in the x, y plane ($\theta = 90^\circ$), the ratio of the maximum intensity to the minimum intensity is ~ 74 [4], however for a molecule aligned in the z axis ($\theta = 0^\circ$), all three channels (0° , 45° , 90°) will measure the same intensities, making the error in φ the largest.

To summarize, both the emission pattern fitting and the 3-detector method can determine the full 3-dimensional orientation of single molecules. The emission pattern fit method can be used to study many single molecules at the same time, with higher accuracy. The 3-detector method can determine the single molecule orientation at more

than 10 times faster time resolution, with compensation of a larger but possibly acceptable error range.

The potential application of the 3-detector method is to study the reorientation dynamics in the glassy state polymer above the glass transition temperature. The results from the former chapters shows that, at $1.1T_g < T < 1.2T_g$ range, the single molecules embedded in the polymer matrix show little translational dynamics. However their orientational dynamics were too fast to detect by the emission pattern fit method. From this point, the 3-detector method maybe a better solution for this task. Its faster time resolution for orientation determination may give more insight into this area.

REFERENCES

1. Ediger, M.D., Spatially Heterogeneous Dynamics in Supercooled Liquids. *Annu. Rev. Phys. Chem.* , 2000. **51**: p. 30.
2. Bartko, A.P. and R.M. Dickson, Imaging Three-Dimensional Single Molecule Orientations. *Journal of Physical Chemistry B*, 1999. **103**(51): p. 5.
3. Saxton, M.J. and K. Jacobson, SINGLE-PARTICLE TRACKING: Applications to Membrane Dynamics. *Annual Review of Biophysics and Biomolecular Structure*, 1997. **26**: p. 27.
4. Fourkas, J.T., Rapid determination of the three-dimensional orientation of single molecules. *Optics Letters*, 2001. **26**(4): p. 3.
5. Donth, E., The Glass Transition. Relaxation Dynamics in Liquids and Disordered Materials. 2001.
6. Ediger, M.D., C.A. Angell, and S.R. Nagel, Supercooled Liquids and Glasses. *J. Phys. Chem.* , 1996. **100**(31): p. 13.
7. Chang, I., et al., Translational and rotational molecular motion in supercooled liquids studied by NMR and forced Rayleigh scattering. *Journal of Non-Crystalline Solids*, 1994. **172-174**: p. 8.
8. Angell, C.A., Spectroscopy Simulation and Scattering, and the Medium Range Order Problem in Glass. *Journal of Non-Crystalline Solids*, 1985. **73**: p. 17.
9. Fujara, F., et al., Translational and rotational diffusion in supercooled orthoterphenyl close to the glass transition. *Z. phys. B*, 1992. **88**(2).
10. Cicerone, M.T. and M.D. Ediger, Photobleaching Technique for Measuring Ultraslow Reorientation near and below the Glass Transition: Tetracene in eTerphenyl. *J. Phys. Chem.*, 1993. **97**(40): p. 9.
11. Stillinger, F.H. and J.A. Hodgdon, Translation-rotation paradox for diffusion in fragile glass-forming liquids. *Physical review E*, 1994. **50**(3): p. 5.
12. Einstein, A., The motion of elements suspended in static liquids as claimed in the molecular kinetic theory of heat. *Annalen Der Physik*, 1905. **17**(8): p. 12.
13. Debye, P., Polar Molecules. 1929.
14. Landau, L.D. and E.M. Lifshitz, Fluid Mechanics. 1987.

15. Cicerone, M.T. and M.D. Ediger, Enhanced translation of probe molecules in supercooled o-terphenyl: Signature of spatially heterogeneous dynamics? *J. Chem. Phys.*, 1996. **104**(18): p. 9.
16. Tarjus, G. and D. Kivelson, Breakdown of the Stokes–Einstein relation in supercooled liquids. *J. Chem. Phys.*, 1995. **103**(8): p. 3.
17. Moerner, W.E. and D.P. Fromm, Methods of single-molecule fluorescence spectroscopy and microscopy. *Review of Scientific Instruments*, 2003. **74**(8): p. 23.
18. Comish, P.V. and T. Ha, A Survey of Single-Molecule Techniques in Chemical Biology. *ACS Chemical Biology*, 2007. **2**(1): p. 9.
19. Schneckenburger, H., Total internal reflection fluorescence microscopy: technical innovations and novel applications. *Current Opinion in Biotechnology*, 2005. **16**(1): p. 6.
20. Ha, T., et al., Probing the interaction between two single molecules: Fluorescence resonance energy transfer between a single donor and a single acceptor. *Proceedings of the National Academy of Sciences of the United States of America*, 1996. **93**: p. 5.
21. Selvin, P.R., The renaissance of fluorescence resonance energy transfer. *nature structural biology*, 2000. **7**(9): p. 5.
22. Yildiz, A., et al., Myosin V Walks Hand-Over-Hand: Single Fluorophore Imaging with 1.5-nm Localization. *Science*, 2003. **300**(5628): p. 5.
23. Ha, T., et al., Single Molecule Dynamics Studied by Polarization Modulation. *Physical Review Letters*, 1996. **77**(19): p. 4.
24. Deschenes, L.A. and D.A.V. Bout, Molecular Motions in Polymer Films near the Glass Transition: a Single Molecule Study of Rotational Dynamics. *J. Phys. Chem. B*, 2001. **105**(48): p. 8.
25. Patra, D., I. Gregor, and J. Enderlein, Image Analysis of Defocused Single-Molecule Images for Three-Dimensional Molecule Orientation Studies. *J. Phys. Chem. A*, 2004. **108**(33): p. 6.
26. Lieb, M.A., J.M. Zavislan, and L. Novotny, Single-molecule orientations determined by direct emission pattern imaging. *J. Opt. Soc. Am. B*, 2004. **21**(6): p. 6.
27. Debarre, A., et al., Quantitative determination of the 3D dipole orientation of single molecules. *Eur. Phys. J. D*, 2004. **28**: p. 11.

28. Hohlbein, J. and C.G. Hubner, Simple scheme for rapid three-dimensional orientation determination of the emission dipole of single molecules. *Applied Physics Letters*, 2005. **86**(12): p. 3.
29. Bartko, A.P. and R.M. Dickson, Three-Dimensional Orientations of Polymer-Bound Single Molecules. *Journal of Physical Chemistry B*, 1999. **103**(16): p. 4.
30. Bartko, A.P., K. Xu, and R.M. Dickson, Three-Dimensional Single Molecule Rotational Diffusion in Glassy State Polymer Films. *Physical Review Letters*, 2002. **89**(2): p. 4.
31. Axelrod, D., T.P. Burghardt, and N.L. Thompson, Total Internal Reflection Fluorescence. *Annual Review of Biophysics and Bioengineering*, 1984. **13**: p. 22.
32. Orts, W.J., et al., Observation of Temperature Dependent Thickness in Ultrathin Polystyrene Films on Silicon. *Physical Review Letters*, 1993. **9**(6): p. 4.
33. Zhu, M., H.A. Hristov, and A.F. Yee, Interface and Surface Effects on the Glass Transition in Thin Polystyrene Films. *Physical Review Letters*, 1997. **78**(8): p. 4.
34. Ellison, C.J. and J.M. Torkelson, Sensing the Glass Transition in Thin and Ultrathin Polymer Films via Fluorescence Probes and Labels. *Journal of Polymer Science Part B: Polymer Physics*, 2002. **40**(24): p. 14.
35. Forrest, J.A., K. Dalnoki-Veress, and J.R. Dutcher, Interface and chain confinement effects on the glass transition temperature of thin polymer films. *Physical review E*, 1997. **56**(5): p. 12.
36. Jain, T.S. and J.J.d. Pablo, Monte Carlo Simulation of Free-Standing Polymer Films near the Glass Transition Temperature. *Macromolecules*, 2002. **35**(6): p. 10.
37. Dalnoki-Veress, K., et al., Molecular weight dependence of reductions in the glass transition temperature of thin, freely standing polymer films. *Physical review E*, 2001. **63**(3): p. 10.
38. Wallace, W.E., J.H.v. Zanten, and W.L. Wu, Influence of an impenetrable interface on a polymer glass-transition temperature. *Physical review E*, 1995. **52**(4): p. 4.
39. Keddie, J.L., R.A.L. Jones, and R.A. Cory, Interface and Surface Effects on the Glass-transition Temperature in Thin Polymer Films. *Faraday Discussions*, 1994. **98**(1): p. 12.

40. Alcoutlabi, M. and G.B. McKenna, Effects of confinement on material behaviour at the nanometre size scale. *Journal of Physics: Condensed Matter*, 2005. **17**: p. 64.
41. Grohens, Y., et al., Tacticity and surface chemistry effects on the glass transition temperature of thin supported PMMA films. *Materials Research Society Symposium*, 2000. **629**: p. 7.
42. McKenna, G.B., Status of our understanding of dynamics in confinement: Perspectives from Confit 2003. *The European Physical Journal E*, 2003. **12**(1): p. 4.
43. Hellen, E.H. and D. Axelrod, Fluorescence Emission at Dielectric and Metal-film Interfaces. *Journal of the Optical Society of America B*, 1987. **4**(3): p. 14.
44. Bartko, A.P., Deciphering Spatially Heterogeneous Polymer Dynamics Using Single Molecule Microscopy. 2002.
45. Qian, H., M.P. Sheetz, and E.L. Elson, Single particle tracking: Analysis of diffusion and flow in two-dimensional systems. *Biophysical Journal*, 1991. **60**(4): p. 12.
46. Wang, C.-Y. and M.D. Ediger, How Long Do Regions of Different Dynamics Persist in Supercooled o-Terphenyl? *J. Phys. Chem. B*, 1999. **103**(20): p. 8.
47. Saxton, M.J., Lateral diffusion in an archipelago Single-particle diffusion. *Biophysical Journal*, 1993. **64**: p. 16.
48. Schob, A., et al., Reorientation and translation of individual dye molecules in a polymer matrix. *European Polymer Journal*, 2004. **40**: p. 8.
49. Weiss, S., Fluorescence Spectroscopy of Single Biomolecules. *Science*, 1999. **283**(5408): p. 8.
50. Hinze, G., G. Diezemann, and T. Basche, Rotational Correlation Functions of Single Molecules. *Physical Review Letters*, 2004. **93**(20): p. 4.
51. Ha, T., et al., Polarization Spectroscopy of Single Fluorescent Molecules. *J. Phys. Chem. B*, 1999. **103**(33): p. 12.
52. Forkey, J.N., M.E. Quinlan, and Y.E. Goldman, Protein structural dynamics by single-molecule fluorescence polarization. *Progress in Biophysics and Molecular Biology* 2000. **74**(1-2): p. 35.

53. Forkey, J.N., M.E. Quinlan, and Y.E. Goldman, Measurement of Single Macromolecule Orientation by Total Internal Reflection Fluorescence Polarization Microscopy. *Biophysical Journal*, 2005. **89**(2): p. 11.